Inferring effective effort in camera trap surveys: a comparison of continuous versus discrete approaches

1 Introduction

Global biodiversity is changing at an unprecedented rate, driving demand for scalable monitoring tools that can operate continuously over large spatial and temporal scales (Fund, 2024; Gonzalez et al., 2023). Passive sensor technologies, such as camera traps and acoustic recorders (Cordier et al., 2022; Priyadarshani et al., 2018), are increasingly being used to meet monitoring demands. Camera traps surveys are widely adopted for wildlife monitoring, deploying an array of cameras within a survey area that automatically record or take images of animals as they pass into a zone of detection (ZOD). They are non-invasive, relatively low-cost, capable of recording multiple species simultaneously, and provide large numbers of multi-species detections in continuous time (Burton et al., 2015; Steenweg et al., 2017).

Camera trap data are used for modelling species distributions or densities, such as within occupancy (Nichols et al., 2008) or capture-recapture (**?**) frameworks that account for false negative detection error (failure to detect the species despite its presence in the study area). However, these models assume that cameras are functioning normally throughout the entire survey. This is not typically the case, as cameras can break or experience battery depletion (Glover-Kapfer et al., 2019). If reduced survey effort due to camera failure is not explicitly modelled, inferred abundances or distributions can be biased because missing detections are incorrectly attributed to ecological processes rather than lost effort (Meek et al., 2014). Cameras are often deployed for several months in remote, difficult-to-access locations, and are not routinely revisited (Buckreus et al., 2021; García-Salgado et al., 2015) so that their working states, and the precise time they failed, are unobserved. Effective effort corresponds to the total survey time during which a camera was functioning normally, analogous to camera-trap days in survey reporting (Meek et al., 2014). This chapter introduces novel modelling frameworks for inferring latent camera working states from detection histories in order to determine the effective effort of each camera.

Each image taken by a camera during the survey contains three pieces of data: (1) spatial data (i.e. GPS coordinates for the camera of each image), (2) temporal data (i.e. date and time when the image was taken), and (3) image labels (such as the species in the image, or whether the image is blank, Bubnicki et al., 2024). However, camera trap data are not without error; this work addresses challenges relating to camera battery failures (Glover-Kapfer et al., 2019), whilst

accounting for sensor malfunction (false positives, Glover-Kapfer et al., 2019). These are both identified by practitioners as considerable constraints in camera trap surveys (at 40% and 42% of survey responses respectively, Glover-Kapfer et al., 2019).

As discussed above, battery depletion leads to un-modelled reduction in effective effort which leads to bias in inferred species abundances or distributions and increases the probability of not making a species detection given its presence in the survey area (false negative error). False negatives refer to the failure to detect the species despite its presence in either the study area or in the ZOD (Palencia et al., 2022). The former definition is typically used in occupancy modelling, whilst the latter may occur due to low camera sensitivity or poor placement. We assume rigorous field protocols are used to minimise the probability of a camera sensor failing to detect an individual in the ZOD (McIntyre et al., 2020; Nakashima et al., 2022). Similarly, we do not separate species presence from detection conditional on presence; therefore, detection rates refer to joint detection probabilities, not detection probabilities given presence in the study area. In this framework, since our inferential target is the latent camera state, false negatives refer to the failure to detect the species due to camera failure, rather than species absence, a point we return to in Section 5.

We define false positives as sensor malfunction leading to blank images (empty images that do not contain an individual), which arise when a sensor triggers in response to anomalous heat signatures in the ZOD (such as waving grasses or reflections of the sun Glover-Kapfer et al., 2019). We do not refer to false positive detections with respect to species misclassification (Zett et al., 2022). High camera trigger sensitivities are often required to reduce the probability of missing a detection in the ZOD, but this also increases the number of blank images (Palencia et al., 2022). A particular type of sensor failure occurs when these become damaged and lead to the sensor continuously and erroneously triggering regardless of the presence or absence of heat signatures in the ZOD. Sensor damage results in an abrupt spike in blank images and typically signals imminent battery failure. Sensor damage inflates the number of blank images, fills memory card space, and drains batteries (Glover-Kapfer et al., 2019).

This chapter develops two modelling frameworks for inferring latent camera working states from detection histories, whilst accounting for false negative and false positives, in order to determine the effective effort of the survey. Under both frameworks, the data are modelled hierarchically, with detection rates and labels conditioned on the latent camera state. The camera can occupy one of three unobserved states (operating normally, battery depletion, or continuously mis-triggering) and transitions between these states are temporally autocorrelated. For example, a camera that is out of battery will remain so till the end of the survey (unless repaired), and a camera that is continuously mis-triggering will quickly run out a battery. Detection rates as well as their labels (i.e blank or species classification) are dependent on the latent camera state. For example, high rates of blank-images are indicative of sensor damage, whilst extended periods without any detections usually indicate battery failure. Modelling these patterns within a hierarchical framework allows us to separate the ecological processes from sensor performance and to reconstruct effective effort for each camera. The two developed models share the framework described above, but differ in their modelling of latent state transitions.

The first framework models these data using a continuous-time Markov modulated marked Poisson process (MMMPP, Mews et al., 2023), which is an extension of the Markov modulated Poisson process (MMPP, Guillera-Arroita et al., 2011; Borchers and Langrock, 2015; Choquet, 2018; Kellner et al., 2022). The second framework is a discrete-time Poisson hidden Markov model (HMM, Mcclintock et al., 2020). In the MMMPP, the latent camera state follows a continuous-time Markov chain, with inter-detection times and detection labels modelled as a state-dependent marked Poisson process. In the Poisson-HMM, the latent camera state evolves at discrete time steps, and for each interval we model the numbers of detections of each label as independent Poisson counts. See Figure 1 for an overview of these processes.

Both the HMM and the MMMPP can be used to infer latent camera states, but our proposed models develop existing approaches. Notably, this work extends current approaches for inferring latent states in MMMPP frameworks. Typically, the Viterbi algorithm is used to infer latent states at detection times only (Mews et al., 2023). We develop this by inferring state probabilities across inter-detection intervals, enabling identification of the camera failure state that is otherwise unobservable using the Viterbi algorithm as this state does not generate detections. Historically, practical solutions to avoid battery failures include setting increased time delays between sensor triggers or the use of solar panels and alternate batteries (Glover-Kapfer et al., 2019), but few statistical approaches exist to account for these when they occur. Similarly, in typical analyses, blank images are often discarded because they do not contain data on the target species (Glover-Kapfer et al., 2019), yet they carry information about the period over which the camera was operational. Our proposed modelling frameworks make use these false positive images to help infer when cameras stopped working.

This chapter also develops the work in Chapter **??**, which investigated continuous versus discrete detection protocols, by extending this comparison to the latent process. Ecological data are often analysed using discrete-time models, developed for observation data collected by human observers during discrete sampling occasions (Pautrel et al., 2024). Whilst discrete-time models are often simple to implement, are generally computationally faster than continuous-time models (Pautrel et al., 2024), and are supported by accessible software (Schofield et al., 2018), the aggregation of continuous detections obscures fine-scale temporal structure and affects model identifiability and interpretation (see Chapter **??**). Continuous-time models avoid discretisation issues and more closely reflect the underlying latent ecological process, but are more complex to implement, less familiar in the ecological literature, and are typically more computationally demanding. In this chapter, we evaluate how these continuous and discrete-time frameworks recover effective effort and detection rates in the presence of camera battery failure and false positive detections.

The work is structured as follows. In Section 2 we introduce the latent camera process, the detection process, the MMMPP and Poisson HMM formulations, and how we define and measure effective effort. In Section 3 we present a simulation study fitting these models under a Bayesian framework and explore model performance over a range of ecological and survey design scenarios and across different levels of temporal discretisation. Finally, in Section 4 we apply both models to a multi-species camera-trap survey in Malaysia, comprising 8076 detections over 121 cameras between May and October 2015, illustrating how effective effort and detection rates can be inferred.

2 Models

In this section, we introduce the statistical models for the HMM and MMMPP mentioned in Section 1 beginning with common aspects between both frameworks. Let n cameras be situated within the study area, where each camera is in place for a total length of time E_i, $i = 1, \cdots, n$. During the survey, the latent camera state $s_{i,\tau}$ at time $\tau \in [0, E_i]$ denotes its operational state. In this work cameras can be operating in one of three states; normal, broken (or non-operational, such as battery depletion), or continuously mis-triggering. We denote these as states 1, 2, and 3 respectively. Over the survey period, each camera can transition between these three states, with the following restrictions:

- The camera always begins the survey by operating normally.
- If a broken camera is repaired (such as battery replacement), it must begin by operating normally.
- If a camera is continuously mis-triggering, it must then transition to broken, representing battery depletion.

If required, further restrictions can be imposed on models under certain camera trap survey designs. For example, where cameras are not revisited and repaired during the survey period, broken cameras must remain broken until camera collection.

We use K_i to denote the total number of images taken by camera i. By convention we will let time zero denote the time at which the cameras are first operational. Each image $k \in \{1, \cdots, K_i\}$ for camera i has a unique timestamp $t_{i,k}$, where $0 < t_{i,1} < \cdots < t_{i,K_i} < E_i$, representing the length of time between set up and image k. The detection times for camera i are recorded in $\mathbf{t_i} = (t_{i,1}, \cdots, t_{i,K_i})$. If $K_i = 0$ then we let $\mathbf{t_i} = \emptyset$.

The rate at which each camera takes images is dependent on its latent state as well as ecological or technical factors. We do not explicitly model the separate processes of animal presence in the ZOD and the probability of detection given presence, and simply model the joint detection rate. However, it is reasonably expected that detection rate will vary across cameras due to these processes, and so we allow for between-camera heterogeneity. Whilst camera i is in state s, the time between consecutive detections is exponentially distributed with rate $\lambda_{i,s}$. In state 2, the camera is broken and so we take $\lambda_{i,2} = 0$ (i.e no detections are possible and so the rate is zero). In state 3, the camera is continuously mis-triggering and so we expect the detection rate to be much higher than in state 1, therefore we assume that $\lambda_{i,3} >> \lambda_{i,1}$.

The detection process may be labelled or 'marked', wherein each image k for camera i is assigned a label (or classification) $\gamma_{i,k}$. Examples of these include species or individual identifications, behaviours, or whether the image is blank or not. For G possible distinct labels then $\gamma_{i,k} \in \{0, \cdots, G-1\}$. The distribution of marks for each detection is conditional on the latent state of the camera. Since this work focuses primarily on inferring the effective effort of each camera and we do not target a focal species, we will label each image according to whether it is a 'true positive'

(containing an image of an individual) or a 'false positive' (no individual can be seen). In this case, we let $\gamma_{i,k} \in \{0, 1\}$ denote whether detection k by camera i is a true positive (1) or a false positive (0).

We assume that camera detections when working normally and mis-triggering are governed by two distinct processes; the first ecological and the second technical. The ecological process determines the rate at which true positive images are taken, i.e the rate at which individuals are present in the ZOD and are detected by the camera. This process is independent of the latent camera state as well as the technical process. The technical process concerns the rate at which false positive (blank) images are taken, which is conditional on the latent camera state. Following this, we impose the following structure on $\lambda_{i,1}$ and $\lambda_{i,3}$ given the underlying process behind the mark generation. Let λ_i^+ denote the rate at which the camera i makes true positive detections. Let $\lambda_{i,1}^-$ and $\lambda_{i,3}^-$ denote the rates at which the camera makes false positive detections in states 1 and 3 respectively. The detection rates can then be expressed as $\lambda_{i,1} = \lambda_i^+ + \lambda_{i,1}^-$ and $\lambda_{i,3} = \lambda_i^+ + \lambda_{i,3}^-$. Given these detection rate decompositions, the probability distribution for image labels can be expressed as:

$$\mathbb{P}(\gamma_{i,k}|s_{i,k} = s) = \begin{cases} \lambda_i^+/\lambda_{i,s} & \text{if } \gamma_{i,k} = 1, \\ \lambda_{i,s}^-/\lambda_{i,s} & \text{otherwise,} \end{cases} \tag{1}$$

for $s_{i,k} = s_{i,t_{i,k}}$ the state of camera i at detection k. Since the number of blank images taken in state 3 is expected to be very high, it follows that $\lambda_{i,3}^- >> \lambda_{i,1}^-$ so that in addition to the rate at which detection are made, the distribution of marks is also indicative of the state the camera is in. In other words, we would expect far more false positives in state 3 than in state 1.

Although in this work we only consider whether an image contains an individual, if species-specific detection rates were required the formulation above could be extended. Setting $g = 1, \cdots, G$ species-detection rates $\lambda_{i,g}^+$, it then follows that $\lambda_i^+ = \sum_{g=1}^G \lambda_{i,g}^+$ and $\mathbb{P}(\gamma_{i,k} = g|s_{i,k} = s) = \lambda_{i,g}^+/\lambda_{i,s}$. Alternatively, the detection process may not be marked and only detection histories $\mathbf{t_i}$ for each camera are recorded. Though we focus on the marked cases, the following models can easily simplified to account for non-marked data. In the un-marked case, inference will target only the state specific detection rates $\lambda_{i,s}$. Finally, though we can allow for the false positive detection rate, $\lambda_{i,3}^-$ to vary by camera, in reality the rate at which cameras continuously mis-trigger is determined by the camera type and the camera settings. Where these are identical across the study, we assume this rate to be homogenous across cameras and use λ_3^- only.

The models in this paper share the latent camera state, detection, and mark processes described above. However, they differ in how these are modelled, in particular whether the latent camera state is expected to evolve in continuous or discrete time.

2.1 Model likelihoods

As discussed in Section 1, the data generated by camera trap surveys can be modelled in discrete time, using an HMM (in Section 2.1.1), or in continuous time, using an MMMPP (in Section 2.1.2).

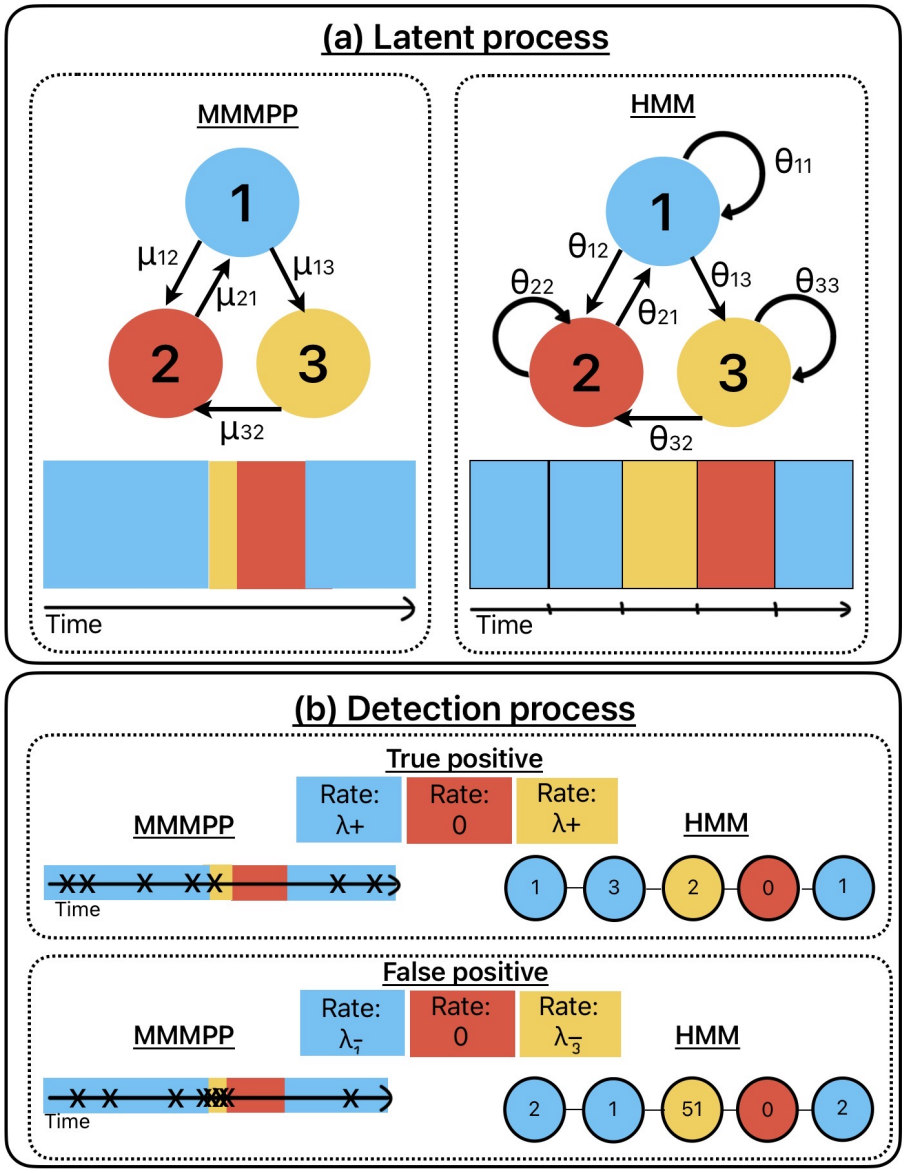

Figure 1: The (a) latent camera state and (b) detection processes for the continuous MMMPP and discrete HMM models. The camera transitions between three states: (1) normal, (2) broken, and (3) mis-triggering. Transition rates are shown for the MMMPP, and transition probabilities are shown for the HMM. An example latent camera state trajectory is shown for both the MMMPP and HMM. Detection rates are modelled conditional on the latent camera state, and are labelled either true or false positive. Example detection histories are shown for both the MMMPP (detection times) and HMM (counts).

2.1.1 Hidden Markov Model (HMM)

In the HMM formulation, the latent camera state evolves discretely in time according to a Markov process. For each camera i, let the survey period of duration E_i be divided into distinct and non-overlapping intervals of duration R, resulting in $P_i = E_i/R$ time-periods. We denote by $s^D_{i,p}, p = 1, \cdots, P_i$, the state of camera i during time-period p. The camera state changes between time-periods can be described by the following probability transition matrix:

$$\Theta = \begin{bmatrix} \theta_{11} & \theta_{12} & \theta_{13} \\ \theta_{21} & \theta_{22} & 0 \\ 0 & \theta_{32} & \theta_{33}, \end{bmatrix}$$

where $\theta_{xy} = \mathbb{P}(s^D_{i,p+1} = y | s^D_{i,p} = x)$ for camera i and time points p. Note that $\theta_{23} = \theta_{31} = 0$ by the transition assumptions defined earlier. The transition matrix for the HMM is presented graphically in the top right of Figure 1.

For the detection process, let $C^1_{i,p}$ and $C^0_{i,p}$ denote the counts of true positive and false positive images, respectively, taken by camera i during time period p. Given the detection rates λ^+_i, $\lambda^-_{i,1}$, and λ^-_3, the counts $C^1_{i,p}$ and $C^0_{i,p}$ are Poisson distributed and for $s^D_{i,p} = s \in \{1, 3\}$ we have the following joint probability distribution:

$$\begin{aligned} \mathbb{P}(C^0_{i,p}, C^1_{i,p} | s^D_{i,p} = s) &= \mathbb{P}(C^0_{i,p} | s^D_{i,p} = s) \mathbb{P}(C^1_{i,p} | s^D_{i,p} = s) \\ &= \frac{(\lambda^-_{i,s})^{C^0_{i,p}} \exp(-\lambda^-_{i,s})}{C^0_{i,p}!} \frac{(\lambda^+_i)^{C^1_{i,p}} \exp(-\lambda^+_i)}{C^1_{i,p}!}, \end{aligned}$$

and for $s^D_{i,p} = 2$ we have:

$$\mathbb{P}(C^0_{i,p}, C^1_{i,p} | s^D_{i,p} = 2) = \begin{cases} 1 & \text{if } C^0_{i,p}, C^1_{i,p} = 0, \\ 0 & \text{otherwise.} \end{cases}$$

The detection process for the HMM is presented graphically in the bottom right of Figure 1. Following the assumption that at the beginning of the survey, all cameras i start by functioning normally, then $s^D_{i,1} = 1$ and the initial camera state distribution is $[1, 0, 0]$. The likelihood function for the camera trap survey data can then be expressed as:

$$\mathcal{L} = \prod_{i=1}^{n} \left\{ [1, 0, 0] \left(\prod_{p=1}^{P_i - 1} \text{diag}(\mathbf{A}_{i,p}) \Theta \right) \text{diag}(\mathbf{A}_{i,P_i}) \mathbf{e} \right\}, \tag{2}$$

where $\mathbf{e}$ is a vector of ones, and entry s of $\mathbf{A}_{i,p}$ denotes $\mathbb{P}(C^0_{i,p}, C^1_{i,p} | s^D_{i,p} = s)$ for $s = 1, 2, 3$.

2.1.2 Markov Modulated Mark Poisson Process (MMMPP)

In the MMMPP formulation, the latent camera state evolves continuously in time according to a continuous-time Markov chain (CTMC). The amount of time spent in each state is exponentially distributed, with the transition rate from state x to state y being μ_{xy}. The latent camera state changes is described by the following transition rate matrix Q:

$$Q = \begin{bmatrix} -\mu_{12} - \mu_{13} & \mu_{12} & \mu_{13} \\ \mu_{21} & -\mu_{21} & 0 \\ 0 & \mu_{32} & -\mu_{32} \end{bmatrix}.$$

Analogously to the HMM, $\mu_{23} = \mu_{31} = 0$ due to the transition assumptions defined earlier. The transition matrix for the MMMPP is presented graphically in the top left of Figure 1. The detection process for the MMMPP can be broken down into the true positive and false positive processes, where observations comprise the time-point of each detection (presented in the bottom left of Figure 1).

Following the assumption that at the beginning of the survey, all cameras i start by functioning normally, then $s_{i,0} = 1$ and the initial camera state distribution is $[1, 0, 0]$. The likelihood function for the camera trap survey data is expressed as:

$$\mathcal{L} = \prod_{i=1}^{n} \left\{ [1,0,0] \left\{ \prod_{k=1}^{K_i} \exp(C[t_{i,k} - t_{i,k-1}]) \Lambda_i \text{diag}(P_{i,k}) \right\} \exp(C[E_i - t_{i,K_i}])\mathbf{e} \right\}, \tag{3}$$

where $t_{i,0} = 0$, $\mathbf{e}$ is a vector of ones, $C = Q - \Lambda$, and $\Lambda = \text{diag}(\lambda_{i,1}, \lambda_{i,2}, \lambda_{i,3})$. If $s_{i,k}$ denotes the state of camera i at detection k, then entry s of $P_{i,k}$ is $\mathbb{P}(\gamma_{i,k}|s_{i,k} = s)$ as defined in Equation 1.

Figure 1 demonstrates the underlying processes for both the MMMPP and HMM models. Note that in the HMM, transitions can only occur between distinct time periods t, whereas transitions may occur at any time in the MMMPP modelling framework. In the MMMPP, the model data are the distances between consecutive detections, whereas in the HMM, model data are counts of detections per time period t.

2.1.3 State at collection

Often in camera trap surveys, whilst the latent camera state is unobserved during the study period this information is often recorded at the end of the survey when the cameras are collected. If camera i is recorded as being in state s at the end of the survey, then in the likelihood equations of 2 and 3 the vector of ones $\mathbf{e}$ can be replaced by $\mathbf{e_s}$, a vector of zeros with a 1 in the s-th entry.

2.1.4 Assumptions

The modelling frameworks above make the following assumptions:

- Detection times and marks are independent of each other, conditional on the latent camera

state.

- Camera transition rates are constant across all cameras in the study. This is a reasonable assumption if all the cameras in the study are of the same type and set up identically. These can be allowed to vary as a function of camera type if necessary.

- Detection rates are allowed to vary between cameras (i.e spatially) and model extensions can consider rates to be functions of spatial covariates. However, detection rates are constant across the study period (i.e temporally). Whilst in the HMM formulation, detection rates can be written as functions of time-period specific covariates, for the MMMPP formulation, finding continuously varying temporal covariates is often difficult.

2.2 Effective effort

Here we show how to infer, at any time-point, the posterior distributions for the latent camera states for both the HMM (Section 2.2.1) and MMMPP (Section 2.2.2). Using these we can then determine posterior distributions for the effective effort of each camera in the survey - defined as the fractional amount of time the camera was able to make detections. We denote by $U_i^s \in (0,1)$ the fractional amount of time that camera i spent in state s over the study period. Therefore U_i^2 is the fraction of time the camera was broken, and $1 - U_i^2$ is the fraction of time that the camera was able to take images (when the camera was in states 1 and 3).

This definition of effective effort is conceptually analogous to the definition of site 'use' or 'availability' probabilities in multi-scale occupancy modelling (Nichols et al., 2008; Emmet et al., 2021; Kellner et al., 2022). In these cases, 'use' reflects the spatial or temporal availability of a species for detection during secondary sampling occasions. In our context, the inferred camera state represents the probability that a camera is capable of making detections during the survey. Whether it is camera operability or species availability that determines if detections are possible, 'effective effort' and 'availability' are both measures of the amount of time during the survey that detections were possible. As such, these are statistically equivalent, and the results that follow apply equally to camera trap surveys as well as multi-scale occupancy data.

2.2.1 HMM

Within a hierarchical Bayesian framework, at each iteration of the MCMC we sample over the latent camera states and can determine the posterior distribution of U_i^s using:

$$U_i^s = \frac{1}{P_i} \sum_{p=1}^{P_i} \mathbb{1}(s_{i,p}^D = s).$$

2.2.2 MMMPP

For the MMMPP, at each iteration of the MCMC, inferring the effective effort of each camera is done in two stages. The first requires that the latent camera state at all detection points be determined.

For a given set of values of transition and detection rates, the Viterbi Algorithm (Mews et al., 2023; Zucchini and MacDonald, 2009) is used to determine the most likely sequence of states $s_{i,t_{i,k}}$ at each time-point $t_{i,k}$ for $k \in \{0, \cdots, K_i + 1\}$, where $t_{i,0} = 0$ and $t_{i,K_i+1} = E_i$, at camera i.

The second stage involves inferring the latent camera state between detection points. Previous approaches to inferring latent states in MMMPP frameworks have relied on the Viterbi algorithm applied only at detection times (Mews et al., 2023). We extend this approach to infer state probabilities across the inter-detection intervals. This extension is essential, as the broken camera state generates no detections and therefore cannot be identified at detection times alone. Instead, its presence can only be inferred from the duration of the intervals between detections. Using the sequence of latent camera states at time-points $t_{i,k}$ for $k \in \{0, \cdots, K_i + 1\}$ from the Viterbi algorithm, we propose the following theorem to determine camera states in the inter-detection periods:

Theorem 1. *Let $s_{i,t}$ be the state of camera i at time-point $t \in (0, E_i)$. By $N^i_{t_1,t_2}$ we denote the number of detections between time-points t_1 and t_2 for camera i. Then for $k \in \{0, \cdots, K_i\}$ and $t \in (t_{i,k}, t_{i,k+1})$:*

$$\mathbb{P}(s_{i,t} = s | s_{i,t_{i,k}} = j_1, s_{i,t_{i,k+1}} = j_2, N^i_{t_{i,k},t_{i,k+1}} = 0) = \frac{\big[\exp(C(t - t_{i,k}))\big]_{j_1,s} \big[\exp(C(t_{i,k+1} - t))\big]_{s,j_2}}{\big[\exp(C(t_{i,k+1} - t_{i,k}))\big]_{j_1,j_2}},$$

where $t_{i,0} = 0$ and $t_{i,K_i+1} = E_i$, $C = Q - \Lambda$ for $\Lambda = diag(\lambda_1, 0, \lambda_3)$, Q is the transition matrix, and $[\mathbf{M}]_{i,j}$ denotes the i,j-th entry of matrix $\mathbf{M}$.

Proof. See Appendix A. □

Using the Viterbi algorithm to determine the $s_{i,t_{i,k}}$ at each time-point $t_{i,k}$ for $k \in \{0, \cdots, K_i+1\}$ and Theorem 1, we can compute U^s_i for camera i and $t \in (0, E_i)$ using:

$$U^s_i = \frac{1}{E_i} \sum_{k=0}^{K_i} \left(\int_{t_{i,k}}^{t_{i,k+1}} \mathbb{P}(s_{i,t} = s | s_{i,t_{i,k}}, s_{i,t_{i,k+1}}, N^i_{t_{i,k},t_{i,k+1}} = 0) dt \right).$$

In reality, this integral is not determined analytically and is instead approximated using numerical integration. For each posterior sample, for some small Δt and $T_i = (t_{i,k+1} - t_{i,k})/\Delta t$ the integral is approximated simply using:

$$\sum_{d=0}^{T_i - 1} \Delta t \mathbb{P}(s_{i,t_{i,k}+d\Delta t} = s | s_{i,t_{i,k}}, s_{i,t_{i,k+1}}, N^i_{t_{i,k},t_{i,k+1}} = 0)$$

3 Simulations

In this Section we investigate inference of the model parameters and the posterior distributions of U^s_i for both model formulations. In particular, we compare how well the HMM (under different levels

Table 1: Simulation scenarios P1 to P4 and the variables that differ between them. Rows show settings for transition rate μ_{21}, and distribution of detection rates λ_i^+ and $\lambda_{i,1}^-$. The Gamma distribution uses the shape/scale parametrisation.

	P1	P2	P3	P4
μ_{21}	$1/50$	0	0	$1/50$
λ_i^+	$\sim$ Gamma$(5, 1/5)$	$\sim$ Gamma$(5, 1/5)$	$\sim$ Gamma$(5, 1/5)$	$\sim$ Gamma$(5, 1/20)$
$\lambda_{i,1}^-$	$\sim$ Gamma$(5, 1/10)$	$\sim$ Gamma$(5, 1/10)$	$\sim$ Gamma$(5, 1/10)$	$\sim$ Gamma$(5, 1/40)$

of temporal discretisation) compares to the MMMPP (the correctly specified model) when data are generated continuously.

We simulate $N = 100$ data sets under four different simulation scenarios denoted P1 to P4 (see Table 1). Each simulation fixes the number of cameras $n = 100$, the length of the study $E_i = 40$, $\mu_{12} = 1/100, \mu_{13} = 1/300, \mu_{32} = 1$, and the mis-triggering detection rate $\lambda_3^- = 100$. The latent state of each camera was also recorded at E_i provided as data to the models. Detection rates for λ_i^+ and $\lambda_{i,1}^-$ are generated from a Gamma distribution to simulate between-camera heterogeneity. On average, we let the true positive detection rates λ_i^+ be twice as high as the false positive detection rates $\lambda_{i,1}^-$. Parameter sets P2 and P3 simulate camera trap survey data in which cameras are not repaired during the survey period (by setting $\mu_{21} = 0$). Parameter set P4 simulates sparse camera trap survey data, with an expected time between true positive images being 4 days (and 8 days for false positive).

Table 2 shows the prior distributions used for each model. Since the detection rates are a common parameter in both the HMM and MMMPP formulations these share the same prior distributions. Prior distributions for transition rates μ_{21} and θ_{21} follow those in Table 2 for simulations P1, P3, and P4. In P2, we set the prior distributions for these transition rates to zero. We do not set this constraint for P3 in order to check model performance under mis-specification. For each data set, a single MCMC chain was run, with $11,000$ iterations, $1,000$ burn-in and thinning of 10.

For the HMM formulation, we consider 5 levels of temporal discretisation. The survey period of duration $E = 40$ is divided into temporal units of duration $R \in \{0.25, 0.5, 1, 2, 4\}$, which results in $P \in \{160, 80, 40, 20, 10\}$ distinct time-periods respectively. These represent discretisations that vary from fine to coarse scale.

3.1 Results

Tables 3 and 4 show results of effective effort, U_i^s, and model parameters, respectively, for each of the HMM models and the MMMPP model. Each table show the mean values, across the 100 simulations, of mean bias (MB), the range (R) of the 95% posterior credible intervals (determined by the 2.5% and 97.5% quantiles of the posterior distribution), and the coverage of the true value (C).

With respect to U_i^s, the MMMPP generally has lower mean bias and narrower credible intervals than the HMM models. The HMM models show that parameter inference differs across choice of

Table 2: Prior distributions used in each model (MMMPP or HMM) for each parameter across the simulation scenarios P1 to P4. The Gamma distribution uses the shape/scale parametrisation.

Model	Parameter	Prior	Simulation
MMMPP and HMM	λ_i^+	$\sim$ Gamma$(1, 5)$	P1-P4
MMMPP and HMM	$\lambda_{i,1}^-$	$\sim$ Gamma$(1, 5)$	P1-P4
MMMPP and HMM	λ_3^-	$\sim$ Gamma$(100, 1)$	P1-P4
MMMPP	μ_{12}	$\sim$ Gamma$(1, 1/100)$	P1-P4
MMMPP	μ_{13}	$\sim$ Gamma$(1, 1/100)$	P1-P4
MMMPP	μ_{21}	$\sim$ Gamma$(1, 1/100)$	P1, P3, P4
MMMPP	μ_{21}	$\mu_{21} = 0$	P2
MMMPP	μ_{32}	$\sim$ Gamma$(1, 1)$	P1-P4
HMM	$(\theta_{11}, \theta_{12}, \theta_{13})$	$\sim$ Dirichlet$(1, 1, 1)$	P1-P4
HMM	$(\theta_{21}, \theta_{22})$	$\sim$ Dirichlet$(1, 1)$	P1, P3, P4
HMM	θ_{21}	$\theta_{21} = 0$	P2
HMM	$(\theta_{32}, \theta_{33})$	$\sim$ Dirichlet$(1, 1)$	P1-P4

discretisation. The smallest discretisations have increased uncertainty, but larger discretisations are too coarse to pick up fine-scale patterns and result in larger bias. Whilst there is a discretisation that minimises bias and uncertainty, this would be difficult to determine a priori, a choice that is avoided when using the MMMPP model. Coverage under the MMMPP is low for simulations P1, P3 and P4. This is due to two factors, the first being that the Viterbi algorithm only determines most probable sequence of states, therefore our inference of the camera states at detections is not fully accounting for all uncertainty. The second factor is that between any two detections, the MMMPP will assign a non-zero probability that the camera is in state 2 (with this probability increasing as the duration between detections increases). This means that the model will almost never assign probability 1 to a state in between detections. When the camera was working normally over an entire survey, the effective effort is 1, but the integration of state probabilities over the survey period cannot be. This is true unless a transition rate is fixed, for example in P2 where $\mu_{21} = 0$ is enforced. In this case the coverage is improved as the inter-detection periods cannot have a broken camera. In P3, the constraint that cameras cannot be repaired is not enforced in the model, and so it is mis-specified. However, bias and uncertainty are comparable between P2 and P3 for all models showing that they are relatively robust to mis-specification. For the HMM models, bias and uncertainty increase considerably when detectability is low (P4), but the MMMPP only shows small increases. Overall, inference of U_i^s generally has lower bias and uncertainty under the MMMPP across the simulation scenarios than the range of HMM models.

With respect to inference of detection rates, Table 4 shows that across the HMM models and MMMPP model are comparable for λ^+ with nominal coverage and low bias. However, the HMM models have much higher bias for the false positive detection rates λ_1^- and λ_3^- than the MMMPP models. This is due to the aggregation of false positive detections into count data over coarse time-scales, particularly when state 3, the mis-triggering state, is a rare and short event. As such it is difficult to accurately differentiate these two rates. All models show a small increase in bias

and uncertainty when detections are sparse. With respect to the camera state transition rates, MMMPP generally has low bias and nominal coverage. There is increased bias and uncertainty for μ_{32}, however this parameter governs transitions from state 3, which is a rare event under our simulation parameters and so this is to be expected. Overall, inference for all detection rates has lower bias and uncertainty under the MMMPP than the HMM models.

3.2 Computation time

All models are implemented in NIMBLE (de Valpine et al., 2017) in R version 4.5.3 (R Core Team, 2025), on a server equipped with an Intel Xeon Platinum 8358 CPU (2.60 GHz) and 540 GB of RAM. Figures 2(a) and 2(b) show the computation time (in minutes) for the MCMC sampling for each of the HMM models and the MMMPP model over the 100 data sets in P1. Figure 2(a) shows computation times for the HMM models with respect to the level of discretisation (from $R = 0.25$ to $R = 4$ resulting in $P = 160$ and $P = 10$ time-points respectively). Figure 2(b) shows the computation times for the MMMPP with respect to the number of detections in the data set. Figure 2 shows that across all levels of temporal discretisation considered here, the HMM is much faster than the MMMPP. The slowest model to fit for the HMM was 16.9 minutes using the $R = 0.25$ time-units, and the fastest MMMPP was 58.6 minutes. We can also see that the HMM computation time scales with the level of discretisation, with finer-scales taking longer. The MMMPP, however, scales with the number of detections in the data set. Whilst the MMMPP has lower bias and uncertainty in its inference of effective effort and model parameters, this comes at considerable computational cost.

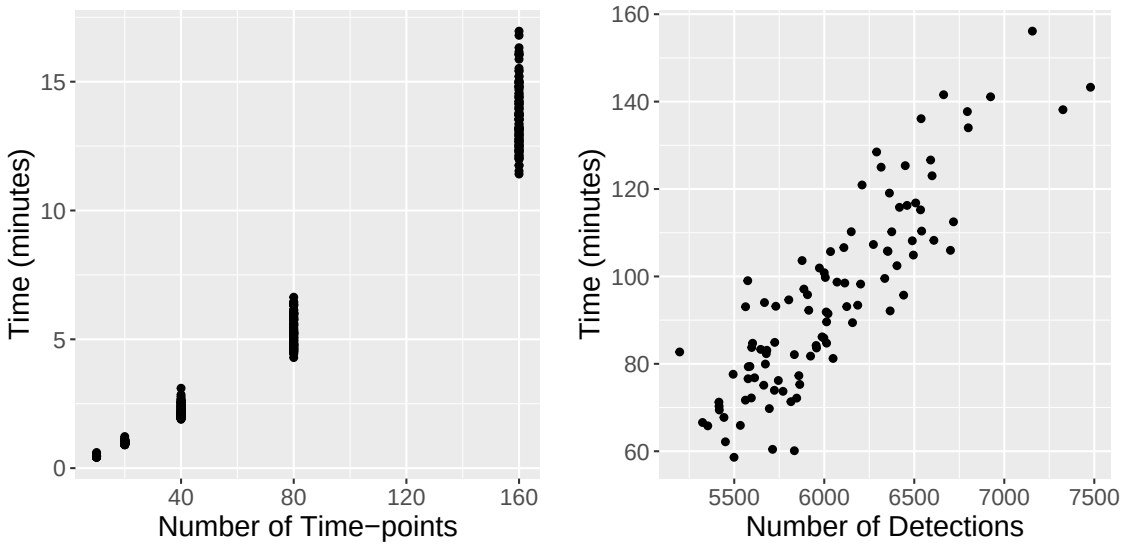

(a) (b)

Figure 2: Computation time (in minutes) for the (a) HMM formulations (across temporal discretisations) and (b) MMMPP formulation (across number of detections)

Table 3: Across simulation settings P1 - P4, and for the MMMPP and HMM models, the table shows mean values of the posterior mean bias (MB), range of 95% credible interval (R), and coverage of the true value (C) for the proportion of time spent in states 1 and 2 (U_i^1 and U_i^2 respectively). The discretisation R for the HMM is denoted in brackets. Also shown are the mean (Mean), upper 95% credible limit (UCL), and lower 95% credible limit (LCL) for the distribution of MSE for U_i^1 and U_i^2.

		P1			P2			P3			P4		
Method	State	MB	R	C	MB	R	C	MB	R	C	MB	R	C
HMM(0.25)	1	-0.004	0.075	0.893	0.005	0.045	0.838	-0.001	0.050	0.852	-0.210	0.318	0.606
HMM(0.5)	1	-0.003	0.062	0.860	0.001	0.024	0.788	-0.001	0.033	0.808	-0.138	0.315	0.701
HMM(1)	1	0.000	0.053	0.796	0.002	0.021	0.725	0.001	0.026	0.744	-0.068	0.297	0.878
HMM(2)	1	0.006	0.042	0.703	0.005	0.019	0.656	0.004	0.021	0.660	-0.046	0.261	0.885
HMM(4)	1	0.019	0.021	0.613	0.013	0.013	0.594	0.013	0.015	0.603	-0.012	0.188	0.796
MMMPP	1	0.001	0.017	0.131	0.001	0.007	0.676	0.000	0.008	0.101	-0.011	0.100	0.215
HMM(0.25)	2	0.005	0.075	0.904	-0.005	0.045	0.829	0.001	0.050	0.857	0.211	0.318	0.614
HMM(0.5)	2	0.003	0.062	0.869	-0.001	0.024	0.784	0.001	0.033	0.811	0.139	0.315	0.710
HMM(1)	2	-0.001	0.053	0.802	-0.003	0.021	0.723	-0.001	0.026	0.747	0.067	0.298	0.892
HMM(2)	2	-0.008	0.042	0.707	-0.007	0.019	0.654	-0.006	0.021	0.662	0.044	0.261	0.897
HMM(4)	2	-0.022	0.020	0.614	-0.017	0.013	0.593	-0.017	0.014	0.603	0.010	0.188	0.805
MMMPP	2	-0.001	0.017	0.130	-0.001	0.007	0.677	-0.000	0.008	0.101	0.011	0.100	0.212
		Mean	UCL	LCL	Mean	UCL	LCL	Mean	UCL	LCL	Mean	UCL	LCL
HMM(0.25)	1	0.004	0.026	0.004	0.003	0.022	0.003	0.002	0.016	0.002	0.125	0.481	0.125
HMM(0.5)	1	0.002	0.012	0.002	0.000	0.003	0.000	0.001	0.004	0.001	0.066	0.302	0.066
HMM(1)	1	0.001	0.011	0.001	0.000	0.003	0.000	0.001	0.004	0.001	0.029	0.160	0.029
HMM(2)	1	0.002	0.013	0.002	0.001	0.005	0.001	0.001	0.005	0.001	0.021	0.126	0.021
HMM(4)	1	0.003	0.028	0.003	0.002	0.011	0.002	0.002	0.011	0.002	0.016	0.102	0.016
MMMPP	1	0.001	0.006	0.001	0.000	0.001	0.000	0.000	0.001	0.000	0.009	0.085	0.009
HMM(0.25)	2	0.004	0.031	0.004	0.003	0.022	0.003	0.003	0.019	0.003	0.126	0.483	0.126
HMM(0.5)	2	0.002	0.013	0.002	0.000	0.003	0.000	0.001	0.005	0.001	0.067	0.304	0.067
HMM(1)	2	0.002	0.011	0.002	0.000	0.003	0.000	0.001	0.004	0.001	0.029	0.161	0.029
HMM(2)	2	0.002	0.012	0.002	0.001	0.004	0.001	0.001	0.004	0.001	0.022	0.127	0.022
HMM(4)	2	0.003	0.026	0.003	0.002	0.009	0.002	0.002	0.009	0.002	0.016	0.101	0.016
MMMPP	2	0.001	0.006	0.001	0.000	0.001	0.000	0.000	0.001	0.000	0.009	0.085	0.009

Table 4: Across simulation settings P1 - P4, and for the MMMPP and HMM models, the table shows the mean values for posterior mean bias (MB), range of 95% credible interval (R), and coverage of the true value (C) for model parameters λ_1^-, λ_3^-, and λ^+. The discretisation R for the HMM is denoted in brackets. Also shown are results for μ_{12}, μ_{13}, μ_{21}, and μ_{32} for the MMMPP.

		P1			P2			P3			P4		
Method	Parameter	MB	R	C	MB	R	C	MB	R	C	MB	R	C
HMM(0.25)	λ_1^-	0.333	0.799	0.932	0.293	0.857	0.927	0.359	0.918	0.931	0.816	0.946	0.802
HMM(0.25)	λ_3^-	-13.492	12.373	0.060	-13.233	11.987	0.060	-13.307	11.793	0.030	-13.704	12.512	0.120
HMM(0.25)	λ^+	0.055	0.818	0.938	0.052	0.915	0.947	0.065	0.920	0.946	0.215	0.737	0.767
HMM(0.5)	λ_1^-	0.274	0.703	0.929	0.367	0.816	0.920	0.337	0.831	0.923	0.688	0.749	0.856
HMM(0.5)	λ_3^-	-23.271	10.760	0.000	-23.690	10.802	0.000	-23.073	10.857	0.000	-24.155	11.644	0.010
HMM(0.5)	λ^+	0.046	0.799	0.943	0.053	0.892	0.946	0.057	0.890	0.949	0.130	0.598	0.855
HMM(1)	λ_1^-	0.256	0.648	0.922	0.363	0.770	0.919	0.357	0.769	0.919	0.454	0.573	0.896
HMM(1)	λ_3^-	-35.208	9.328	0.000	-37.952	8.843	0.000	-36.927	8.968	0.000	-37.069	9.513	0.000
HMM(1)	λ^+	0.034	0.772	0.944	0.040	0.854	0.947	0.040	0.848	0.952	0.078	0.509	0.929
HMM(2)	λ_1^-	0.253	0.621	0.917	0.388	0.741	0.914	0.376	0.737	0.915	0.413	0.497	0.894
HMM(2)	λ_3^-	-50.087	7.669	0.020	-52.566	7.405	0.010	-52.964	7.259	0.000	-51.676	8.298	0.010
HMM(2)	λ^+	0.014	0.737	0.944	0.016	0.802	0.944	0.017	0.799	0.950	0.059	0.455	0.943
HMM(4)	λ_1^-	0.254	0.588	0.905	0.417	0.696	0.901	0.394	0.684	0.904	0.370	0.425	0.886
HMM(4)	λ_3^-	-63.320	6.199	0.020	-60.819	8.163	0.070	-62.587	6.718	0.030	-58.522	9.922	0.100
HMM(4)	λ^+	-0.017	0.695	0.931	-0.017	0.745	0.929	-0.017	0.741	0.937	0.037	0.400	0.949
MMMPP	λ_1^-	0.056	0.620	0.951	0.090	0.778	0.947	0.083	0.750	0.949	0.095	0.540	0.947
MMMPP	λ_3^-	-0.265	12.205	0.980	0.498	12.217	0.970	0.229	11.998	0.960	-0.051	12.288	1.000
MMMPP	λ^+	0.050	0.827	0.946	0.076	0.979	0.946	0.073	0.960	0.948	0.092	0.633	0.946
MMMPP	μ_{12}	-0.000	0.007	0.950	0.000	0.007	0.940	0.000	0.007	0.980	0.002	0.010	0.890
MMMPP	μ_{13}	0.000	0.004	0.940	0.000	0.004	0.940	0.000	0.004	0.970	0.000	0.004	0.970
MMMPP	μ_{21}	-0.001	0.021	0.960	0.000	0.000	1.000	0.001	0.005	0.000	0.003	0.029	0.990
MMMPP	μ_{32}	0.075	1.283	0.930	0.082	1.265	0.980	0.048	1.241	0.940	0.131	1.327	0.960

4 Malaysian camera trap survey

We apply both the MMMPP and HMM models to a camera trap survey data set from Sabah, Malaysia in order to compare posteriors for our primary inferential target - effective effort. The data set includes $n = 121$ cameras, set up on average for 44.4 days (minimum 33.8 days, maximum 97.9 days), between May and October 2015. The cameras in the study trigger when an anomalous heat signature crosses into the ZOD, producing a series of 10 images taken at 1 second intervals. To define a unique detection, the time of the first image in the sequence was used as the detection time-stamp, and if a species was detected in any of the 10 images, then this was the species label given to that detection. If no individual was detected across the sequence, then the image was classed as a false positive. We assume that detections are independent and follow recommendations that impose an 'independence threshold' of 30 minutes (Ridout and Linkie, 2009) (though other intervals can reach up to an hour, Bahaa-el din et al., 2016) within which repeat detections of the same species are discarded to account for individuals resting in front of the camera for extended periods. Failure to impose this independence condition can result in artificially inflated detection rates which are the result of repeated detections of the same individual encounter rather than increased species activity or abundance at that camera. This assumption is discussion further in Section 5. Detections of novel species or blank images within the time threshold are not discarded.

In this survey, all but three of the cameras took time-lapse photos at 10am every day; for cameras that were non-operational at camera collection, an inspection of its detection history reveals a 24-hour window between time-lapses (or between the last detection and next scheduled time-lapse) during which the camera may have broken.

Across the 121 cameras, there were a total of 8076 detections, comprising 2380 true positives and 5696 false positives. Camera 'EA-VJR1' comprises two detection histories ((A) and (B)) as the camera was installed during two separate sampling occasions. Table 5 shows a summary of the detections for cameras that broke during the survey period, with the total number of true positive images, false positive images (blanks), the number of days the camera was in situ (E_i), and the minimum and maximum number of camera-trap nights (CTNs). Table 8 provides these same details for all cameras in the survey. The CTN minimum is determined by the time at which the last detection or time-lapse was made, and the maximum is when the camera failed to register its next daily time-lapse. In total, 25 cameras were broken at time of collection. Table 5 shows a significant amount of between-camera heterogeneity in detection rates for both λ_i^+ and $\lambda_{1,i}^-$. Additionally, cameras 'EA-VJR1(B)' and 'EA-VJR5' show a considerable number of blank images (1162 and 1447 respectively), which may indicate sensor damage and camera mis-triggering.

The time-lapses from this survey, and the subsequent ranges of effective effort for malfunctioning cameras, allow us to compare inferred effective effort from the HMM and MMMPP modelling frameworks. During the survey cameras were not revisited so for the MMMPP we take $\mu_{21} = 0$, and in the HMMs we take $\theta_{21} = 0$. We allow for between camera heterogeneity in detection rates λ_+ and λ_-^1, but assume that λ_-^3 is shared across cameras. One camera was removed from the survey, 'EA-VJR1(B)', due to a violation in the modelling assumptions that prevented model fitting in the

Table 5: For each of the 121 cameras in the survey, the table provides the number of images containing an individual (TP), blank images (FP), the number of days the camera was in situ (E_i), and an estimate (maximum and minimum) of the number of camera trap nights (CTNs) for cameras which were non-operational at collection.

ID	TP	FP	E_i	CTNs
CLF-17	45	8	42.00	[22.42,22.99]
CLF-R5	1	1	42.00	[0.09,0.81]
EA-A1	3	0	47.10	[11.96,12.96]
EA-C1	21	102	97.95	[78.02,79.02]
EA-VJR1 (A)	22	13	85.04	[35.96,36.95]
EA-VJR1 (B)	13	1162	42.00	[8.73,8.91]
EA-VJR5	51	1447	42.00	[33.96,34.95]
EA-VJR8	7	1	42.00	[32.84,33.84]
OP-27	0	1	42.00	[4.75,4.81]
OP-25	4	1	45.00	[14.76,14.83]
OP-24	0	0	43.00	[0,0.87]
OP-16	11	2	43.00	[8.91,9.91]
OP-13	2	1	43.00	[28.74,29.74]
OP-8	1	6	45.00	[17.81,18.81]
OP-7	2	0	42.00	[2.99,3.77]
OP-2	2	2	42.00	[8.89,9.89]
OP-1	3	7	47.00	[10.84,11.84]
OP-OP3	0	9	45.00	[8.96,9.96]
OPF-10	10	8	43.00	[17.35,18.01]
OPF-8	4	286	46.00	[35.04,35.86]
OPF-HCV9	12	2	42.00	[27.96,28.96]
OPF-HCV12	3	1	73.00	[9.01,10.01]
OPF-R5	4	0	45.00	[8.88,9.88]
OPF-RR2	1	0	42.00	[3.79,4.79]
OPF-RR16	3	1	45.00	[7.99,8.99]

MMMPP; the detection histories showed that after a period of high intensity of false positive images there were subsequent short burst interspersed by periods of no detections before camera battery depletion. This is a violation of the assumption that high intensity is followed by battery depletion, which we return to in Section 5. All cameras are assumed to start in state 1, and we allow the model to know the state of the camera at collection as this information was recorded. The time-lapse detection histories were removed from the data so that model performance can be generalised to surveys in which cameras do not record these. The data are analysed according to the MMMPP formulation as well as the HMM with temporal-units of duration $R = 0.5$, 1, and 2 days. Model priors and MCMC details are given in Appendix B.2.

4.1 Results

Figure 3 shows the posterior means and 95% credible intervals for the effective effort of each of the 24 cameras that broke during the survey. The black bars show the naive minimum and maximum estimates effective effort based on the detection histories and time-lapses from Table 5. The MMMPP shows, in general, narrower intervals than the HMM models. The amount of uncertainty across all models increases as the number of detections at each camera decreases. For example, OP-24 and OP-27 have the greatest uncertainty in each model and have 0 and 1 total detections respectively. In each model, inference of effective effort is supported by the sharing of latent state transition rates across cameras in the survey. Figure 3 also shows that the inferred effective effort differs across levels of discretisation. The temporal units here, of lengths $R = 0.5$, 1, and 2 days, give reasonably comparable values; however more extreme units, such as $R = 0.25$ or $R = 4$ days may see increased bias and uncertainty.

Tables 6 and 7 show the posterior means and 95% credible intervals for cameras that broke during the survey across each model for true positive and false positive detection rates respectively. Tables 10 and 11 give the same for all cameras in the survey. Generally, for most cameras the inferred posterior distributions are comparable across models (and HMM discretisations). Where these differ more considerably is across cameras with low detection rates and cameras that broke during the survey period. For example, true positive detection rates differ for cameras OP-24 and CLF-R5 across model formulations, where these cameras totalled 0 and 2 detections each and broke within one day of camera set up. These same patterns hold true for each camera concerning the false positive detection rates. However, whilst the true positive detection rates are largely robust across the choice of discretisation in the HMM (when cameras did not break), the same is not true in general of the false positive detection rates. The true positive detection rate is constant across normal camera function and the mis-triggering state. The false positive detection rates do differ across these latent camera states, and so choice of discretisation is more influential. For example, camera EA-VJR5 (in which the camera experienced a sensor malfunction with greatly inflated number of blank images) sees considerable variation in the false positive detection rate. HMM(0.5) has posterior mean 0.27, HMM(1) has mean 2.38, and the MMMPP has mean 0.4. In this case, the time-period intervals divide or aggregate detection histories differently and false positives from the mis-triggering state can be falsely attributed to false positives when the camera is functioning normally. This can also be seen from the false positive detection rate λ_3^- from Table 7, which differs considerably across choice of temporal discretisation. Whilst the false positives are generally nuisances, the incorrect attribution of false positive detection rates according to state can subsequently affect inferred effective effort at each camera. In general, the MMMPP avoids bias that arises due to the choice of discretisation as data are modelled in continuous time.

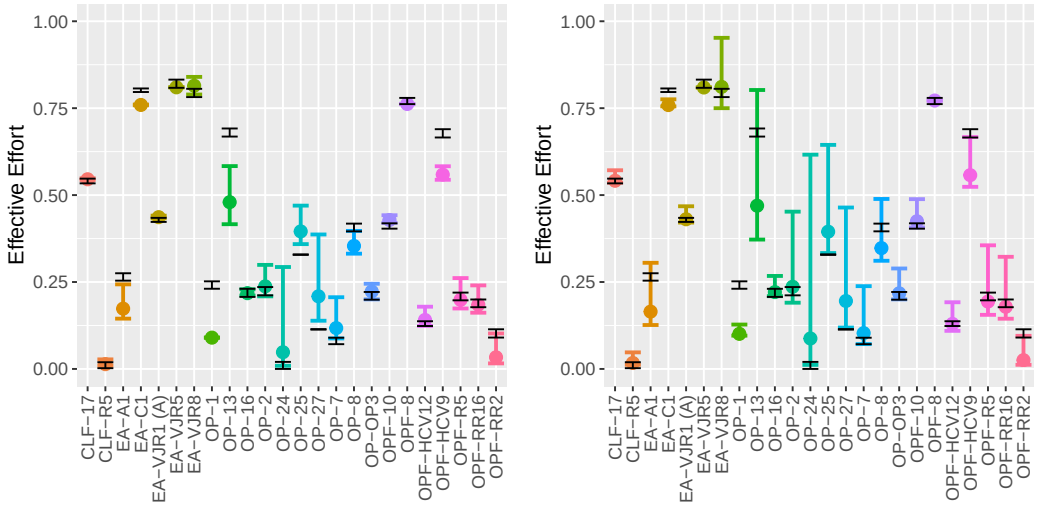

(a) MMMPP

(b) HMM(0.5)

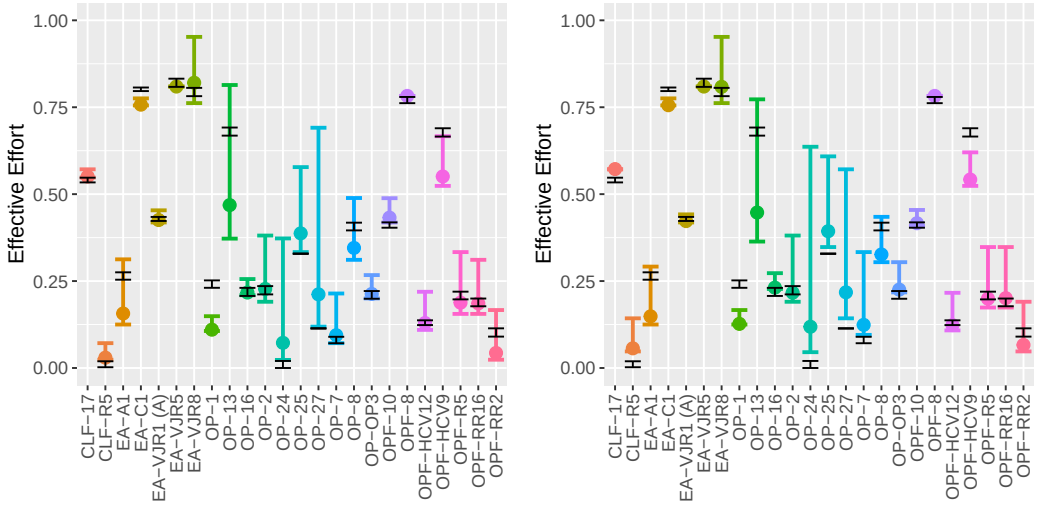

(c) HMM(1)

(d) HMM(2)

Figure 3: Posterior means and 95% credible intervals for $U_i^1 + U_i^3$, the fractional amount of time the camera was capable of taking images, for the (a) MMMPP and HMMs (at (b) $R = 0.5$, (c) 1, and (d) 2 respectively). Black bars show the minimum and maximum effective effort determined by the detection histories and time-lapse data from each camera.

5 Discussion

Camera trap surveys are widely used in ecological monitoring as they passively collect large volumes of species detections with minimal human interference. These data provide information on which

Table 6: Posterior means and 95% credible intervals for true positive detection rates λ_i^+ for broken cameras from models HMM ($R = 0.5$, 1 and 2) and the MMMPP.

Camera	HMM(0.5)	HMM(1)	HMM(2)	MMMPP
CLF-17	1.94 (1.41, 2.53)	1.9 (1.39, 2.52)	1.84 (1.34, 2.43)	1.93 (1.41, 2.54)
CLF-R5	1.23 (0.14, 3.65)	0.95 (0.1, 2.7)	0.61 (0.08, 1.74)	1.54 (0.17, 4.36)
EA-A1	0.48 (0.12, 1.1)	0.49 (0.13, 1.14)	0.52 (0.13, 1.22)	0.47 (0.12, 1.06)
EA-C1	0.29 (0.18, 0.42)	0.29 (0.18, 0.42)	0.29 (0.18, 0.43)	0.29 (0.18, 0.42)
EA-VJR1(A)	0.61 (0.38, 0.89)	0.61 (0.39, 0.9)	0.61 (0.38, 0.9)	0.61 (0.39, 0.89)
EA-VJR5	1.48 (1.1, 1.91)	1.48 (1.12, 1.93)	1.49 (1.11, 1.92)	1.49 (1.13, 1.92)
EA-VJR8	0.23 (0.1, 0.41)	0.23 (0.1, 0.41)	0.23 (0.1, 0.42)	0.23 (0.1, 0.43)
OP-27	0.12 (0, 0.49)	0.12 (0, 0.5)	0.11 (0, 0.42)	0.12 (0, 0.47)
OP-25	0.28 (0.08, 0.61)	0.28 (0.09, 0.62)	0.26 (0.08, 0.55)	0.27 (0.08, 0.56)
OP-24	0.43 (0.01, 2.04)	0.35 (0.01, 1.51)	0.25 (0, 1.06)	0.65 (0.01, 2.88)
OP-16	1.16 (0.59, 1.9)	1.16 (0.6, 1.91)	1.08 (0.55, 1.75)	1.17 (0.58, 1.92)
OP-8	0.12 (0.01, 0.35)	0.12 (0.01, 0.34)	0.13 (0.01, 0.34)	0.12 (0.01, 0.34)
OP-7	0.62 (0.11, 1.59)	0.65 (0.12, 1.65)	0.53 (0.09, 1.39)	0.58 (0.1, 1.48)
OP-2	0.29 (0.05, 0.72)	0.29 (0.06, 0.72)	0.31 (0.06, 0.75)	0.28 (0.06, 0.7)
OP-1	0.7 (0.2, 1.54)	0.64 (0.18, 1.41)	0.56 (0.14, 1.27)	0.8 (0.21, 1.76)
OP-OP3	0.1 (0, 0.36)	0.1 (0, 0.36)	0.09 (0, 0.35)	0.1 (0, 0.37)
OPF-10	0.57 (0.28, 0.95)	0.56 (0.28, 0.94)	0.57 (0.28, 0.98)	0.57 (0.29, 0.95)
OPF-8	0.14 (0.04, 0.28)	0.13 (0.05, 0.27)	0.14 (0.04, 0.28)	0.14 (0.04, 0.28)
OPF-HCV9	0.54 (0.28, 0.89)	0.54 (0.28, 0.89)	0.55 (0.29, 0.9)	0.54 (0.28, 0.87)
OPF-HCV12	0.39 (0.1, 0.88)	0.4 (0.1, 0.9)	0.41 (0.1, 0.92)	0.38 (0.09, 0.83)
OPF-R5	0.54 (0.15, 1.13)	0.56 (0.16, 1.18)	0.51 (0.14, 1.07)	0.53 (0.15, 1.11)
OPF-RR2	1.1 (0.11, 3.3)	0.87 (0.08, 2.61)	0.6 (0.06, 1.75)	1.09 (0.11, 3.31)
OPF-RR16	0.46 (0.12, 1.03)	0.44 (0.11, 1)	0.41 (0.11, 0.95)	0.46 (0.11, 1.04)

species were detected at specific locations and times, and are therefore commonly used in occupancy and abundance models. However, camera trap data are subject to several sources of error. In this work, our primary inferential target was effective camera effort, modelled whilst explicitly accounting for camera battery malfunction, and false positive detections (blank images). We develop two modelling frameworks for camera trap data to achieve this, using either continuous (MMMPP-Markov modulated marked Poisson process) or discrete-time (HMM - hidden Markov model with Poisson counts) latent processes. Of interest was whether the fully continuous-time framework (MMMPP) offers substantial inferential advantages over the discrete-time Poisson HMM for inferring species detection rates and effective camera effort in the presence of battery failures and sensor malfunctions.

Both approaches model the data hierarchically and allow inference on the latent camera states throughout the survey, but exhibit different strengths and limitations. Simulation results show that the Poisson–HMM can achieve low bias and uncertainty in estimates of detection rates and effective effort at relatively low computational cost. However, its performance depends strongly on the choice of temporal discretisation. During simulations, the MMMPP generally showed smaller bias and uncertainty than the HMM formulations whilst avoiding the need for arbitrary discretisation, but

Table 7: Posterior means and 95% credible intervals for false positive detection rates $\lambda_{i,1}^-$ (for broken cameras) and λ_3^- from models HMM ($R = 0.5$, 1 and 2) and the MMMPP.

Camera	HMM(0.5)	HMM(1)	HMM(2)	MMMPP
CLF-17	0.39 (0.18, 0.69)	0.39 (0.18, 0.68)	0.37 (0.17, 0.64)	0.39 (0.18, 0.69)
CLF-R5	2.5 (0.24, 7.56)	1.5 (0.18, 4.41)	0.85 (0.09, 2.49)	4.51 (0.44, 14.5)
EA-A1	0.14 (0, 0.53)	0.14 (0, 0.53)	0.14 (0, 0.55)	0.14 (0, 0.51)
EA-C1	1.38 (1.12, 1.66)	1.38 (1.13, 1.66)	1.39 (1.14, 1.68)	1.38 (1.12, 1.65)
EA-VJR1(A)	0.38 (0.21, 0.61)	0.38 (0.21, 0.61)	0.38 (0.21, 0.61)	0.38 (0.21, 0.61)
EA-VJR5	0.27 (0.12, 0.48)	2.38 (1.88, 2.94)	0.28 (0.13, 0.5)	0.4 (0.21, 0.64)
EA-VJR8	0.06 (0.01, 0.16)	0.06 (0.01, 0.16)	0.06 (0.01, 0.16)	0.06 (0.01, 0.16)
OP-27	0.28 (0.03, 0.84)	0.27 (0.02, 0.86)	0.26 (0.03, 0.84)	0.27 (0.03, 0.86)
OP-25	0.12 (0.01, 0.34)	0.11 (0.01, 0.32)	0.11 (0.01, 0.31)	0.12 (0.01, 0.33)
OP-24	0.73 (0.01, 3.6)	0.56 (0.01, 2.48)	0.32 (0, 1.43)	1.78 (0.01, 9.41)
OP-16	0.31 (0.07, 0.76)	0.32 (0.07, 0.76)	0.29 (0.06, 0.68)	0.32 (0.07, 0.77)
OP-8	0.45 (0.17, 0.87)	0.45 (0.18, 0.85)	0.48 (0.18, 0.9)	0.45 (0.17, 0.85)
OP-7	0.24 (0.01, 0.92)	0.27 (0.01, 1.02)	0.21 (0, 0.81)	0.24 (0.01, 0.94)
OP-2	0.31 (0.06, 0.77)	0.32 (0.07, 0.82)	0.33 (0.07, 0.82)	0.3 (0.06, 0.74)
OP-1	1.62 (0.7, 2.97)	1.5 (0.63, 2.72)	1.27 (0.51, 2.34)	0.94 (0.26, 2.07)
OP-OP3	1.01 (0.48, 1.75)	1.02 (0.47, 1.8)	0.95 (0.43, 1.62)	0.98 (0.42, 1.71)
OPF-10	0.49 (0.23, 0.86)	0.48 (0.22, 0.84)	0.49 (0.23, 0.86)	0.49 (0.21, 0.87)
OPF-8	8.03 (7.14, 8.92)	7.96 (7.07, 8.9)	7.93 (7.07, 8.87)	8.14 (7.22, 9.12)
OPF-HCV9	0.13 (0.03, 0.3)	0.13 (0.03, 0.32)	0.13 (0.03, 0.32)	0.13 (0.03, 0.31)
OPF-HCV12	0.21 (0.03, 0.62)	0.22 (0.03, 0.64)	0.22 (0.03, 0.64)	0.2 (0.02, 0.6)
OPF-R5	0.11 (0, 0.42)	0.12 (0, 0.46)	0.11 (0, 0.43)	0.11 (0, 0.42)
OPF-RR2	1.06 (0.02, 4.42)	0.7 (0.02, 2.82)	0.38 (0.01, 1.49)	1.03 (0.01, 4.19)
OPF-RR16	0.25 (0.03, 0.74)	0.25 (0.03, 0.73)	0.22 (0.02, 0.64)	0.26 (0.03, 0.73)
λ_3^-	895 (858, 933)	1083(1037,1129)	746 (716, 777)	1069(1025,1113)

these differences depended strongly on the choice of temporal discretisation in the HMM, with some discretisations performing similarly to the MMMPP. Furthermore, the reduced bias and uncertainty in the MMMPP come at a cost of increased computation cost and model complexity.

Although we allowed for between-camera heterogeneity, we did not explicitly model this using covariates. Camera-specific covariates could readily be incorporated when available, but time-varying covariates present additional challenges. In continuous-time models, covariates are often incorporated by dividing the survey period into non-overlapping intervals and assigning covariate values within each interval (Choquet, 2018). This approach allows both detection rates and transition rates to vary over time but increases computational cost (Kellner et al., 2022). Moreover, continuous-time formulations ideally require continuously varying covariates, which are often unavailable in practice. Further work using time-heterogeneous intensity functions within the MMMPP can be considered (Gonçalves et al., 2022; Kellner et al., 2022). In contrast, the discrete HMM formulation allows covariates to be incorporated directly at each time unit with little additional computational burden.

We assume that a camera that begins mis-triggering must eventually transition to a broken state and cannot return to normal function. Although this assumption may not always hold in

practice, it is required within this modelling framework to maintain the Markov property governing state transitions. If cameras could return to normal operation after mis-triggering, the probability of transitioning to the broken state would depend on the previous malfunction history, violating the Markov assumption. If such temporary sensor malfunctions are common, the model could be extended to include an additional latent state representing a "recent repair" condition. In this state, detection rates would match those of the normal functioning state, but transition rates to the broken state would differ. However, introducing additional latent states increases model complexity and may require substantially more data to ensure identifiability.

We have shown that this framework can recover when cameras were broken and unbiased detection rates. However, we did not explicitly account for false negatives due to species absence, which are typically required in occupancy models for example to distinguish between true absence and presence but non-detection. Future work remains to integrate the proposed models formally into wider occupancy frameworks with the aim of conditioning on species presence to distinguishing between non-detection of a species due to non-availability and non-detection due to camera non-functionality.

A major practical limitation of the MMMPP in this study was computational cost. Improving sampling efficiency was not the primary focus of this work, but recent Bayesian implementations have proposed methods that substantially improve computational performance (Gonçalves et al., 2022; Luo and Sherlock, 2025). Future work will explore these approaches. Additionally, the two-stage procedure used here to infer latent camera states—sampling model parameters, applying the Viterbi algorithm to infer states at detection times, and then imputing states between detections—does not fully propagate uncertainty. The methods proposed by (Luo and Sherlock, 2025) may allow a fully integrated inference framework that accounts for this uncertainty.

Simulation results generally indicated that the MMMPP produced lower bias and uncertainty than the HMM formulations. However, these differences depended strongly on the choice of discretisation in the HMM, with some discretisations performing similarly to the MMMPP. In the case study, detection rate estimates from the MMMPP and HMM were comparable for cameras with relatively high detection rates that did not experience malfunction. Larger differences arose for cameras that malfunctioned, particularly those with sensor mis-triggering. In these cases, inferred detection rates varied substantially among HMM models depending on discretisation, whereas the MMMPP avoided this issue. Similarly, the MMMPP produced lower uncertainty in estimates of effective camera effort.

Despite these advantages, the MMMPP proved considerably more sensitive to violations of modelling assumptions. The MMMPP is sensitive to the assumption that cameras must break following mis-triggering. In the case study, one camera detection history had to be removed because it displayed interspersed bursts of mis-triggering before battery depletion. Since the assumption is that mis-triggering can only be followed by battery depletion, the model could not be fitted. The MMMPP is also sensitive to violations of the independence of detections. The enforcement of the independence threshold was required to ensure that repeat detections of the same individual are removed to account for them resting in front of the camera. These repeat detections are a form of self-excitation in the detection histories, wherein a detection increases the chance another detection

will be made shortly. The MMMPP cannot account for this process, and instead will instead increase camera true positive detection rates. This however has the unintended consequence of the model assigning high probability the camera is broken in inter-detection time-intervals. As discussed above, the addition of more latent states to account for the self-excitation behaviour can be considered, but may risk identifiability concerns if confounded with the mis-triggering state. The HMM was less sensitive to such violations because the aggregation of detection times into counts obscures fine-scale temporal patterns. By contrast, the continuous-time model directly captures these patterns, making deviations from model assumptions more evident. The MMMPP was also sensitive to the choice of initial MCMC values in the case study, with poor initialisation preventing likelihood evaluation and hindering mixing. This issue was not observed for the HMM with this dataset.

Our previous work in Chapter **??** demonstrated a strong preference for continuous detection protocols over discrete protocols when using discrete-time latent state models. In this chapter, we find that, for the specific goal of recovering detection rates and effective camera effort under camera failures and mis-triggering, the inferential benefit of a fully continuous-time model over a discrete-time Poisson HMM is not so clear. Although the MMMPP avoids discretisation and provides slightly lower bias and uncertainty, these gains were modest relative to the substantial increase in computational cost and sensitivity to assumption violations. One potential avenue for future work is extending the Δ metric proposed in Chapter **??** to models with multiple discrete latent states. Such an approach could help address one of the primary limitations of discrete-time models, the choice of discretisation. Continuous-time formulations may nonetheless offer greater benefits when fine-scale temporal dynamics are of primary interest, for example when inferring species interactions (Kellner et al., 2022), as these details are inevitably smoothed over when detections are aggregated into discrete intervals in the HMM. Finally, ongoing developments in MMMPP methodology aimed at improving computational efficiency and modelling flexibility may further enhance the practical applicability of continuous-time approaches.

Finally, our definition of effective camera effort is conceptually equivalent to site 'use' or 'availability' (or small-scale occupancy) probabilities in multi-scale occupancy models (Nichols et al., 2008; Emmet et al., 2021). The MMMPP formulation has been used by Kellner et al. (2022) to measure the availability of the species for detection during camera trap surveys (attributing this to species absence rather than camera functionality). In both cases, these represent the probability of availability to make detections during the sampling period. By explicitly modelling these availability processes, we avoid confounding true non-detection (due to absence or malfunction) with ecological signal, yielding unbiased detection rates. This statistical equivalence implies that our MMMPP and Poisson-HMM frameworks apply equally to multi-scale occupancy data as to camera trap surveys. Whilst this work has focused on camera traps, the approaches generalise to other continuous-time passive monitoring datasets, such as acoustic surveys, where similar equipment malfunctions are likely to occur.

Appendix A Proof for Theorem 1

Recall that $[\exp(C(t_{i,k+1} - t_{i,k}))]_{j_1,j_2} = \mathbb{P}(s_{i,t_{i,k+1}} = j_2, N^i_{t_{i,k},t_{i,k+1}} = 0 | s_{i,t_{i,k}} = j_1)$. Then we can show that:

$$\begin{aligned}
&\mathbb{P}(s_{i,t_{i,k}} = j_1, s_{i,t_{i,k+1}} = j_2, N^i_{t_{i,k},t_{i,k+1}} = 0) \\
&\quad = \mathbb{P}(s_{i,t_{k+1}} = j_2, N^i_{t_{i,k},t_{i,k+1}} = 0 | s_{i,t_{i,k}} = j_1)\mathbb{P}(s_{i,t_{i,k}} = j_1) \\
&\quad = [\exp(C(s_{i,t_{i,k+1}} - s_{i,t_{i,k}})]_{j_1,j_2}\mathbb{P}(s_{i,t_{i,k}} = j_1).
\end{aligned}$$

Similarly we can show that:

$$\begin{aligned}
&\mathbb{P}(s_{i,t} = s, s_{i,t_{i,k}} = j_1, s_{i,t_{i,k+1}} = j_2, N^i_{t_{i,k},t_{i,k+1}} = 0) \\
&\quad = \mathbb{P}(N^i_{t,t_{i,k+1}} = 0 | s_{i,t} = s, s_{i,t_{i,k+1}} = j_2)\mathbb{P}(N^i_{t_{i,k},t} = 0 | s_{i,t_{i,k}} = j_1, s_{i,t} = s) \\
&\qquad \mathbb{P}(s_{i,t_{i,k+1}} = j_2 | s_{i,t} = s)\mathbb{P}(s_{i,t} = s | s_{i,t_{i,k}} = j_1)\mathbb{P}(s_{i,t_{i,k}} = j_1) \\
&\quad = \mathbb{P}(s_{i,t_{i,k+1}} = j_2, N^i_{t,t_{i,k+1}} = 0 | s_{i,t} = s)\mathbb{P}(s_{i,t} = s, N^i_{t,t_{i,k}} = 0 | s_{i,t_{i,k}} = j_1) \\
&\qquad \mathbb{P}(s_{i,t_{i,k}} = j_1) \\
&\quad = [\exp(C(t_{i,k+1} - t))]_{s,j_2}[\exp(C(t - t_{i,k}))]_{j_1,s}\mathbb{P}(s_{i,t_{i,k}} = j_1)
\end{aligned}$$

Dividing the probabilities appropriately gives the result.

Appendix B Malaysian camera trap survey data

B.1 Camera details

Table 8 shows a summary of the detections for cameras that broke during the survey period, with the total number of true positive images, false positive images (blanks), the number of days the camera was in situ (E_i), and for cameras that broke during the survey, the minimum and maximum number of camera-trap nights (CTNs).

Table 8: For each of the 121 cameras in the survey, the table provides the number of images containing an individual (TP), blank images (FP), the number of days the camera was in situ (E_i), and an estimate (maximum and minimum) of the number of camera trap nights (CTNs) for cameras which were non-operational at collection. Missing values simply denote the camera was functional throughout the entire survey.

ID	TP	FP	E_i	CTNs
CLF-19	22	2	42.03	
CLF-18	26	7	42.01	
CLF-17	45	8	42.00	[22.42,22.99]
CLF-16	27	9	41.98	

Continued on next page

ID	TP	FP	E_i	CTNs
CLF-14	40	13	42.07	
CLF-12	14	0	42.12	
CLF-11	22	14	42.17	
CLF-10	36	8	42.05	
CLF-9	12	3	42.84	
CLF-8	6	0	41.97	
CLF-7	35	6	41.98	
CLF-6	41	5	41.96	
CLF-5	28	9	41.95	
CLF-4	26	4	41.93	
CLF-3	34	6	42.03	
CLF-2	17	4	42.09	
CLF-1	55	4	41.86	
CLF-LFE	19	3	42.89	
CLF-LFER	20	3	55.83	
CLF-R1	94	17	41.94	
CLF-R2	42	6	42.02	
CLF-R3	5	3	42.82	
CLF-R4	23	0	42.85	
CLF-R5	1	1	42.00	[0.09,0.81]
CLF-R6	34	41	42.08	
CLF-R8	61	11	41.94	
EA-A1	3	0	47.10	[11.96,12.96]
EA-A10	7	1	46.98	
EA-A100	5	0	47.07	
EA-B1	35	17	47.08	
EA-B10	10	4	47.08	
EA-B100	13	2	47.02	
EA-C1	21	102	97.95	[78.02,79.02]
EA-C10	17	1	41.99	
EA-C100	12	24	41.92	
EA-D1	31	6	43.03	
EA-D10	11	3	43.01	
EA-D100	35	5	42.85	
EA-E1	15	5	42.68	
EA-E10	27	3	42.93	
EA-E100	39	5	42.83	
EA-F1	18	14	42.04	

Continued on next page

ID	TP	FP	E_i	CTNs
EA-F10	13	5	41.95	
EA-F100	6	1	41.92	
EA-R0	9	6	42.17	
EA-R1	16	8	41.99	
EA-R2	32	7	40.97	
EA-R5	3	2	42.96	
EA-R6	19	4	43.01	
EA-R15	21	1	41.94	
EA-R30	9	4	41.95	
EA-R60	20	7	42.10	
EA-R120	4	0	48.05	
EA-VJR1 (A)	22	13	85.04	[35.96,36.95]
EA-VJR1 (B)	13	1162	42.00	[8.73,8.91]
EA-VJR2	9	3	44.98	
EA-VJR3	52	302	42.00	
EA-VJR4	16	1	41.91	
EA-VJR5	51	1447	42.00	[33.96,34.95]
EA-VJR6	47	5	42.00	
EA-VJR7	22	158	41.77	
EA-VJR8	7	1	42.00	[32.84,33.84]
EA-VJRR	26	4	45.03	
OP-31	6	2	41.99	
OP-29	4	67	42.02	
OP-28	7	364	42.08	
OP-27	0	1	42.00	[4.75,4.81]
OP-26 (A)	29	5	34.96	
OP-26 (B)	0	98	33.84	
OP-25	4	1	45.00	[14.76,14.83]
OP-24	0	0	43.00	[0,0.87]
OP-23	1	196	73.03	
OP-22	11	11	43.22	
OP-20	12	204	43.23	
OP-19	26	13	43.07	
OP-18	4	32	46.80	
OP-16	11	2	43.00	[8.91,9.91]
OP-13	2	1	43.00	[28.74,29.74]
OP-12	8	361	42.17	
OP-11	14	2	42.19	

Continued on next page

ID	TP	FP	E_i	CTNs
OP-10	14	12	42.20	
OP-9	20	10	42.06	
OP-8	1	6	45.00	[17.81,18.81]
OP-7	2	0	42.00	[2.99,3.77]
OP-6	11	34	43.21	
OP-5	8	95	42.21	
OP-4	15	103	42.22	
OP-2	2	2	42.00	[8.89,9.89]
OP-1	3	7	47.00	[10.84,11.84]
OP-OP2	7	5	45.00	
OP-OP3	0	9	45.00	[8.96,9.96]
OPF-10	10	8	43.00	[17.35,18.01]
OPF-8	4	286	46.00	[35.04,35.86]
OPF-7	6	1	42.01	
OPF-6	10	5	41.76	
OPF-4	44	7	41.94	
OPF-3	61	26	41.95	
OPF-2	22	6	41.95	
OPF-1	23	11	46.27	
OPF-HCV1	27	8	41.92	
OPF-HCV2	16	3	41.99	
OPF-HCV3	13	15	41.99	
OPF-HCV4	48	4	41.89	
OPF-HCV5	33	12	41.85	
OPF-HCV6	32	38	41.83	
OPF-HCV7	30	5	41.97	
OPF-HCV8	30	13	41.98	
OPF-HCV9	12	2	42.00	[27.96,28.96]
OPF-HCV11	29	7	41.97	
OPF-HCV12	3	1	73.00	[9.01,10.01]
OPF-HCV13	57	12	41.89	
OPF-HCV15	29	4	73.11	
OPF-R1	17	2	41.78	
OPF-R2	8	0	42.12	
OPF-R4	8	10	40.01	
OPF-R5	4	0	45.00	[8.88,9.88]
OPF-R6	37	8	46.84	
OPF-RR2	1	0	42.00	[3.79,4.79]

Continued on next page

ID	TP	FP	E_i	CTNs
OPF-RR3	9	2	41.90	
OPF-RR7	10	1	43.17	
OPF-RR14	21	35	43.23	
OPF-RR16	3	1	45.00	[7.99,8.99]

B.2 MCMC details

Table 9 gives the prior distributions for model parameters in the MMMPP and HMM models. For each model fitting, 3 chains of $11,000$ iterations were run, using $1,000$ burn-in and thinning of 10.

The choice initial values for the chains in the MMMPP was important, as poor choices start the chains in areas of zero-valued likelihoods and prevented the chains from mixing. In this case study, the detection rate parameters were the most influential in resulting in successful mixing, and starting values were determined by naively inspecting the numbers of true and false positive detections for each camera. The sensitivity to the initial conditions was absent in the HMM formulation.

Convergence and mixing was assessed using the Gelman-Rubin diagnostic (all parameters recording values < 1.1) and chains run until an effective sample size of > 2000 values was reached.

Table 9: Prior distributions used in the analysis of the Malaysian camera trap survey data. The Gamma distribution uses the shape/scale parametrisation.

Model	Parameter	Prior
MMMPP and HMM	λ_i^+	$\sim$ Gamma$(1,1)$
MMMPP and HMM	$\lambda_{i,1}^-$	$\sim$ Gamma$(1,5)$
MMMPP and HMM	λ_3^-	$\sim$ Gamma$(800,1)$
MMMPP	μ_{12}	$\sim$ Gamma$(1,1/100)$
MMMPP	μ_{13}	$\sim$ Gamma$(1,1/100)$
MMMPP	μ_{21}	$\mu_{21} = 0$
MMMPP	μ_{32}	$\sim$ Gamma$(1,1)$
HMM	$(\theta_{11}, \theta_{12}, \theta_{13})$	$\sim$ Dirichlet$(1,1,1)$
HMM	$(\theta_{21}, \theta_{22})$	$\theta_{21} = 0$
HMM	$(\theta_{32}, \theta_{33})$	$\sim$ Dirichlet$(1,1)$

B.3 Additional results

Tables 10 and 11 give the posterior means and 95% credible intervals for true positive (λ^+) and false positive ($\lambda_{i,1}^-$ and λ_3^-) detection rates respectively for each camera from models HMM ($R = 0.5$, 1 and 2) and the MMMPP.

Table 10: Posterior means and 95% credible intervals for true positive detection rates λ_i^+ for each camera from models HMM ($R = 0.5$, 1 and 2) and the MMMPP.

Camera	HMM(0.5)	HMM(1)	HMM(2)	MMMPP
CLF-19	0.53 (0.34, 0.77)	0.53 (0.34, 0.78)	0.53 (0.34, 0.77)	0.54 (0.33, 0.78)
CLF-18	0.62 (0.41, 0.88)	0.62 (0.41, 0.88)	0.63 (0.42, 0.89)	0.63 (0.42, 0.9)
CLF-17	1.94 (1.41, 2.53)	1.9 (1.39, 2.52)	1.84 (1.34, 2.43)	1.93 (1.41, 2.54)
CLF-16	0.65 (0.43, 0.92)	0.65 (0.44, 0.91)	0.65 (0.44, 0.91)	0.65 (0.43, 0.91)
CLF-14	0.95 (0.69, 1.27)	0.95 (0.67, 1.26)	0.95 (0.68, 1.25)	0.95 (0.68, 1.27)
CLF-12	0.34 (0.19, 0.54)	0.35 (0.19, 0.55)	0.35 (0.19, 0.54)	0.35 (0.2, 0.55)
CLF-11	0.53 (0.34, 0.79)	0.53 (0.33, 0.77)	0.53 (0.34, 0.77)	0.53 (0.34, 0.76)
CLF-10	0.86 (0.61, 1.15)	0.86 (0.6, 1.15)	0.86 (0.6, 1.16)	0.86 (0.61, 1.17)
CLF-9	0.3 (0.16, 0.48)	0.3 (0.16, 0.48)	0.3 (0.16, 0.47)	0.29 (0.16, 0.47)
CLF-8	0.16 (0.07, 0.3)	0.16 (0.06, 0.31)	0.16 (0.07, 0.31)	0.16 (0.06, 0.31)
CLF-7	0.84 (0.6, 1.13)	0.84 (0.59, 1.13)	0.84 (0.58, 1.15)	0.84 (0.59, 1.11)
CLF-6	0.98 (0.7, 1.29)	0.98 (0.71, 1.3)	0.97 (0.7, 1.28)	0.98 (0.7, 1.32)
CLF-5	0.67 (0.45, 0.94)	0.68 (0.46, 0.94)	0.68 (0.45, 0.94)	0.67 (0.45, 0.94)
CLF-4	0.63 (0.42, 0.89)	0.63 (0.42, 0.89)	0.63 (0.41, 0.88)	0.63 (0.41, 0.9)
CLF-3	0.81 (0.57, 1.1)	0.81 (0.57, 1.11)	0.82 (0.56, 1.11)	0.81 (0.57, 1.11)
CLF-2	0.42 (0.25, 0.63)	0.42 (0.25, 0.64)	0.42 (0.26, 0.64)	0.42 (0.25, 0.63)
CLF-1	1.31 (0.99, 1.68)	1.31 (0.98, 1.68)	1.3 (0.99, 1.67)	1.31 (0.99, 1.68)
CLF-LFE	0.46 (0.28, 0.68)	0.46 (0.28, 0.68)	0.46 (0.28, 0.68)	0.45 (0.28, 0.67)
CLF-LFER	0.37 (0.23, 0.55)	0.37 (0.23, 0.55)	0.37 (0.23, 0.54)	0.37 (0.23, 0.54)
CLF-R1	2.21 (1.78, 2.68)	2.21 (1.79, 2.69)	2.21 (1.8, 2.68)	2.22 (1.81, 2.65)
CLF-R2	1 (0.72, 1.31)	1 (0.72, 1.3)	1 (0.72, 1.31)	1 (0.72, 1.32)
CLF-R3	0.14 (0.05, 0.26)	0.14 (0.05, 0.26)	0.14 (0.05, 0.27)	0.14 (0.05, 0.27)
CLF-R4	0.55 (0.35, 0.78)	0.55 (0.35, 0.8)	0.55 (0.35, 0.78)	0.55 (0.35, 0.79)
CLF-R5	1.23 (0.14, 3.65)	0.95 (0.1, 2.7)	0.61 (0.08, 1.74)	1.54 (0.17, 4.36)
CLF-R6	0.8 (0.56, 1.1)	0.81 (0.57, 1.09)	0.81 (0.56, 1.1)	0.81 (0.57, 1.11)
CLF-R8	1.44 (1.09, 1.82)	1.44 (1.1, 1.81)	1.45 (1.1, 1.82)	1.45 (1.1, 1.83)
EA-A1	0.48 (0.12, 1.1)	0.49 (0.13, 1.14)	0.52 (0.13, 1.22)	0.47 (0.12, 1.06)
EA-A10	0.17 (0.07, 0.3)	0.17 (0.07, 0.31)	0.17 (0.07, 0.31)	0.16 (0.07, 0.3)
EA-A100	0.13 (0.05, 0.25)	0.12 (0.05, 0.24)	0.12 (0.05, 0.24)	0.12 (0.05, 0.24)
EA-B1	0.75 (0.53, 1.02)	0.75 (0.53, 1.02)	0.75 (0.53, 1.01)	0.75 (0.53, 1.02)
EA-B10	0.23 (0.11, 0.38)	0.23 (0.11, 0.38)	0.23 (0.11, 0.38)	0.23 (0.11, 0.38)
EA-B100	0.29 (0.16, 0.46)	0.29 (0.16, 0.46)	0.29 (0.16, 0.46)	0.29 (0.16, 0.46)
EA-C1	0.29 (0.18, 0.42)	0.29 (0.18, 0.42)	0.29 (0.18, 0.43)	0.29 (0.18, 0.42)
EA-C10	0.41 (0.24, 0.63)	0.42 (0.25, 0.63)	0.42 (0.25, 0.63)	0.42 (0.24, 0.63)
EA-C100	0.3 (0.16, 0.49)	0.3 (0.15, 0.5)	0.3 (0.16, 0.48)	0.3 (0.16, 0.49)

Continued on next page

Camera	HMM(0.5)	HMM(1)	HMM(2)	MMMPP
EA-D1	0.73 (0.5, 1)	0.73 (0.49, 1.01)	0.73 (0.5, 1)	0.73 (0.51, 1)
EA-D10	0.27 (0.14, 0.44)	0.27 (0.14, 0.44)	0.27 (0.14, 0.45)	0.27 (0.14, 0.44)
EA-D100	0.82 (0.58, 1.11)	0.82 (0.57, 1.11)	0.82 (0.57, 1.12)	0.82 (0.58, 1.11)
EA-E1	0.37 (0.21, 0.56)	0.37 (0.21, 0.58)	0.37 (0.21, 0.56)	0.37 (0.2, 0.56)
EA-E10	0.64 (0.42, 0.89)	0.63 (0.42, 0.89)	0.64 (0.42, 0.9)	0.64 (0.43, 0.9)
EA-E100	0.91 (0.65, 1.22)	0.92 (0.66, 1.21)	0.91 (0.66, 1.22)	0.91 (0.65, 1.21)
EA-F1	0.44 (0.27, 0.66)	0.44 (0.27, 0.67)	0.44 (0.27, 0.66)	0.44 (0.26, 0.66)
EA-F10	0.33 (0.18, 0.53)	0.32 (0.18, 0.52)	0.33 (0.18, 0.52)	0.32 (0.18, 0.51)
EA-F100	0.16 (0.07, 0.31)	0.16 (0.07, 0.31)	0.16 (0.07, 0.3)	0.16 (0.06, 0.3)
EA-R0	0.23 (0.11, 0.38)	0.23 (0.11, 0.4)	0.23 (0.11, 0.4)	0.23 (0.11, 0.4)
EA-R1	0.4 (0.23, 0.61)	0.39 (0.23, 0.6)	0.4 (0.23, 0.61)	0.4 (0.23, 0.61)
EA-R2	0.79 (0.56, 1.08)	0.79 (0.54, 1.08)	0.79 (0.54, 1.07)	0.78 (0.54, 1.07)
EA-R5	0.09 (0.03, 0.2)	0.09 (0.03, 0.2)	0.09 (0.03, 0.2)	0.09 (0.03, 0.2)
EA-R6	0.45 (0.28, 0.68)	0.45 (0.28, 0.67)	0.46 (0.28, 0.67)	0.45 (0.28, 0.66)
EA-R15	0.51 (0.32, 0.75)	0.51 (0.32, 0.76)	0.52 (0.32, 0.76)	0.51 (0.32, 0.74)
EA-R30	0.23 (0.11, 0.4)	0.23 (0.11, 0.39)	0.23 (0.11, 0.4)	0.23 (0.11, 0.4)
EA-R60	0.49 (0.3, 0.72)	0.49 (0.3, 0.72)	0.49 (0.31, 0.73)	0.49 (0.3, 0.72)
EA-R120	0.1 (0.03, 0.2)	0.1 (0.03, 0.21)	0.1 (0.04, 0.21)	0.1 (0.03, 0.21)
EA-VJR1(A)	0.61 (0.38, 0.89)	0.61 (0.39, 0.9)	0.61 (0.38, 0.9)	0.61 (0.39, 0.89)
EA-VJR2	0.22 (0.11, 0.37)	0.22 (0.11, 0.36)	0.22 (0.11, 0.37)	0.22 (0.11, 0.37)
EA-VJR3	1.24 (0.92, 1.58)	1.23 (0.93, 1.59)	1.23 (0.91, 1.58)	1.23 (0.93, 1.58)
EA-VJR4	0.4 (0.23, 0.61)	0.4 (0.23, 0.62)	0.39 (0.23, 0.6)	0.4 (0.23, 0.6)
EA-VJR5	1.48 (1.1, 1.91)	1.48 (1.12, 1.93)	1.49 (1.11, 1.92)	1.49 (1.13, 1.92)
EA-VJR6	1.12 (0.82, 1.44)	1.12 (0.83, 1.46)	1.12 (0.82, 1.44)	1.12 (0.82, 1.45)
EA-VJR7	0.54 (0.34, 0.77)	0.53 (0.34, 0.77)	0.54 (0.34, 0.78)	0.54 (0.35, 0.79)
EA-VJR8	0.23 (0.1, 0.41)	0.23 (0.1, 0.41)	0.23 (0.1, 0.42)	0.23 (0.1, 0.43)
EA-VJRR	0.59 (0.39, 0.82)	0.59 (0.39, 0.82)	0.59 (0.38, 0.83)	0.59 (0.39, 0.83)
OP-31	0.16 (0.07, 0.3)	0.16 (0.06, 0.3)	0.16 (0.07, 0.31)	0.16 (0.06, 0.3)
OP-29	0.12 (0.04, 0.24)	0.12 (0.04, 0.23)	0.12 (0.04, 0.24)	0.12 (0.04, 0.24)
OP-28	0.19 (0.08, 0.34)	0.19 (0.08, 0.33)	0.19 (0.08, 0.33)	0.18 (0.08, 0.33)
OP-27	0.12 (0, 0.49)	0.12 (0, 0.5)	0.11 (0, 0.42)	0.12 (0, 0.47)
OP-26 (A)	0.84 (0.57, 1.17)	0.83 (0.55, 1.16)	0.83 (0.55, 1.16)	0.83 (0.57, 1.15)
OP-26 (B)	0.03 (0, 0.1)	0.03 (0, 0.11)	0.03 (0, 0.11)	0.03 (0, 0.11)
OP-25	0.28 (0.08, 0.61)	0.28 (0.09, 0.62)	0.26 (0.08, 0.55)	0.27 (0.08, 0.56)
OP-24	0.43 (0.01, 2.04)	0.35 (0.01, 1.51)	0.25 (0, 1.06)	0.65 (0.01, 2.88)
OP-23	0.03 (0, 0.08)	0.03 (0, 0.08)	0.03 (0, 0.08)	0.03 (0, 0.07)
OP-22	0.27 (0.14, 0.44)	0.27 (0.14, 0.44)	0.27 (0.14, 0.44)	0.27 (0.14, 0.45)
OP-20	0.29 (0.16, 0.47)	0.29 (0.15, 0.46)	0.29 (0.16, 0.47)	0.29 (0.16, 0.47)

Continued on next page

Camera	HMM(0.5)	HMM(1)	HMM(2)	MMMPP
OP-19	0.61 (0.4, 0.86)	0.61 (0.4, 0.87)	0.62 (0.41, 0.86)	0.61 (0.4, 0.87)
OP-18	0.1 (0.03, 0.22)	0.1 (0.04, 0.21)	0.1 (0.04, 0.21)	0.1 (0.03, 0.21)
OP-16	1.16 (0.59, 1.9)	1.16 (0.6, 1.91)	1.08 (0.55, 1.75)	1.17 (0.58, 1.92)
OP-13	0.15 (0.03, 0.37)	0.15 (0.03, 0.38)	0.15 (0.03, 0.38)	0.14 (0.03, 0.35)
OP-12	0.21 (0.1, 0.36)	0.21 (0.1, 0.37)	0.21 (0.1, 0.36)	0.21 (0.09, 0.36)
OP-11	0.35 (0.2, 0.56)	0.35 (0.19, 0.54)	0.35 (0.19, 0.56)	0.34 (0.19, 0.53)
OP-10	0.35 (0.2, 0.54)	0.35 (0.19, 0.54)	0.35 (0.19, 0.55)	0.35 (0.19, 0.54)
OP-9	0.48 (0.3, 0.71)	0.49 (0.31, 0.71)	0.49 (0.31, 0.72)	0.49 (0.3, 0.72)
OP-8	0.12 (0.01, 0.35)	0.12 (0.01, 0.34)	0.13 (0.01, 0.34)	0.12 (0.01, 0.34)
OP-7	0.62 (0.11, 1.59)	0.65 (0.12, 1.65)	0.53 (0.09, 1.39)	0.58 (0.1, 1.48)
OP-6	0.27 (0.14, 0.44)	0.27 (0.14, 0.45)	0.27 (0.14, 0.44)	0.28 (0.14, 0.44)
OP-5	0.21 (0.1, 0.36)	0.21 (0.1, 0.35)	0.21 (0.1, 0.37)	0.21 (0.1, 0.36)
OP-4	0.37 (0.21, 0.57)	0.37 (0.22, 0.57)	0.37 (0.21, 0.57)	0.37 (0.21, 0.57)
OP-2	0.29 (0.05, 0.72)	0.29 (0.06, 0.72)	0.31 (0.06, 0.75)	0.28 (0.06, 0.7)
OP-1	0.7 (0.2, 1.54)	0.64 (0.18, 1.41)	0.56 (0.14, 1.27)	0.8 (0.21, 1.76)
OP-OP2	0.17 (0.07, 0.32)	0.17 (0.08, 0.31)	0.17 (0.07, 0.31)	0.17 (0.07, 0.31)
OP-OP3	0.1 (0, 0.36)	0.1 (0, 0.36)	0.09 (0, 0.35)	0.1 (0, 0.37)
OPF-10	0.57 (0.28, 0.95)	0.56 (0.28, 0.94)	0.57 (0.28, 0.98)	0.57 (0.29, 0.95)
OPF-8	0.14 (0.04, 0.28)	0.13 (0.05, 0.27)	0.14 (0.04, 0.28)	0.14 (0.04, 0.28)
OPF-7	0.16 (0.06, 0.3)	0.16 (0.07, 0.31)	0.17 (0.07, 0.31)	0.16 (0.07, 0.31)
OPF-6	0.26 (0.13, 0.43)	0.26 (0.13, 0.43)	0.26 (0.12, 0.44)	0.26 (0.13, 0.43)
OPF-4	1.05 (0.76, 1.37)	1.05 (0.76, 1.37)	1.06 (0.77, 1.37)	1.05 (0.76, 1.39)
OPF-3	1.44 (1.1, 1.82)	1.45 (1.12, 1.81)	1.44 (1.1, 1.82)	1.45 (1.12, 1.84)
OPF-2	0.53 (0.33, 0.77)	0.53 (0.34, 0.78)	0.54 (0.34, 0.78)	0.54 (0.33, 0.78)
OPF-1	0.5 (0.32, 0.73)	0.51 (0.33, 0.73)	0.51 (0.33, 0.74)	0.51 (0.33, 0.74)
OPF-HCV1	0.65 (0.44, 0.93)	0.65 (0.43, 0.91)	0.65 (0.44, 0.92)	0.65 (0.44, 0.91)
OPF-HCV2	0.4 (0.24, 0.61)	0.39 (0.23, 0.6)	0.39 (0.23, 0.61)	0.4 (0.24, 0.61)
OPF-HCV3	0.33 (0.18, 0.52)	0.33 (0.18, 0.52)	0.32 (0.18, 0.51)	0.33 (0.18, 0.53)
OPF-HCV4	1.14 (0.85, 1.48)	1.14 (0.85, 1.48)	1.15 (0.85, 1.49)	1.14 (0.84, 1.46)
OPF-HCV5	0.79 (0.55, 1.08)	0.79 (0.56, 1.07)	0.79 (0.55, 1.07)	0.79 (0.55, 1.08)
OPF-HCV6	0.77 (0.53, 1.05)	0.77 (0.53, 1.05)	0.77 (0.52, 1.05)	0.77 (0.52, 1.06)
OPF-HCV7	0.72 (0.48, 0.99)	0.72 (0.49, 1)	0.72 (0.49, 0.98)	0.72 (0.5, 1)
OPF-HCV8	0.72 (0.48, 0.99)	0.72 (0.5, 1.01)	0.72 (0.49, 0.99)	0.72 (0.48, 1)
OPF-HCV9	0.54 (0.28, 0.89)	0.54 (0.28, 0.89)	0.55 (0.29, 0.9)	0.54 (0.28, 0.87)
OPF-HCV11	0.7 (0.47, 0.96)	0.7 (0.48, 0.97)	0.7 (0.47, 0.96)	0.7 (0.46, 0.97)
OPF-HCV12	0.39 (0.1, 0.88)	0.4 (0.1, 0.9)	0.41 (0.1, 0.92)	0.38 (0.09, 0.83)
OPF-HCV13	1.35 (1.03, 1.72)	1.35 (1.02, 1.73)	1.36 (1.03, 1.74)	1.36 (1.03, 1.71)
OPF-HCV15	0.41 (0.27, 0.56)	0.41 (0.27, 0.57)	0.41 (0.27, 0.56)	0.4 (0.27, 0.55)

Continued on next page

Camera	HMM(0.5)	HMM(1)	HMM(2)	MMMPP
OPF-R1	0.42 (0.25, 0.63)	0.42 (0.25, 0.64)	0.42 (0.24, 0.64)	0.42 (0.24, 0.63)
OPF-R2	0.21 (0.1, 0.36)	0.21 (0.1, 0.37)	0.21 (0.1, 0.36)	0.21 (0.1, 0.36)
OPF-R4	0.22 (0.1, 0.38)	0.22 (0.1, 0.38)	0.22 (0.1, 0.38)	0.22 (0.1, 0.38)
OPF-R5	0.54 (0.15, 1.13)	0.56 (0.16, 1.18)	0.51 (0.14, 1.07)	0.53 (0.15, 1.11)
OPF-R6	0.79 (0.56, 1.07)	0.79 (0.56, 1.08)	0.8 (0.56, 1.06)	0.8 (0.56, 1.08)
OPF-RR2	1.1 (0.11, 3.3)	0.87 (0.08, 2.61)	0.6 (0.06, 1.75)	1.09 (0.11, 3.31)
OPF-RR3	0.23 (0.11, 0.4)	0.23 (0.11, 0.4)	0.23 (0.11, 0.4)	0.23 (0.12, 0.4)
OPF-RR7	0.25 (0.12, 0.42)	0.25 (0.12, 0.42)	0.25 (0.13, 0.41)	0.25 (0.12, 0.41)
OPF-RR14	0.5 (0.31, 0.73)	0.5 (0.32, 0.73)	0.5 (0.32, 0.72)	0.5 (0.31, 0.73)
OPF-RR16	0.46 (0.12, 1.03)	0.44 (0.11, 1)	0.41 (0.11, 0.95)	0.46 (0.11, 1.04)

Table 11: Posterior means and 95% credible intervals for false positive detection rates λ_i^- (for each camera) and λ_3^- from models HMM ($R = 0.5$, 1 and 2) and the MMMPP.

Camera	HMM(0.5)	HMM(1)	HMM(2)	MMMPP
CLF-19	0.07 (0.01, 0.17)	0.07 (0.02, 0.17)	0.07 (0.01, 0.17)	0.07 (0.02, 0.17)
CLF-18	0.19 (0.08, 0.34)	0.19 (0.08, 0.34)	0.19 (0.08, 0.35)	0.19 (0.08, 0.34)
CLF-17	0.39 (0.18, 0.69)	0.39 (0.18, 0.68)	0.37 (0.17, 0.64)	0.39 (0.18, 0.69)
CLF-16	0.23 (0.11, 0.4)	0.24 (0.12, 0.4)	0.24 (0.11, 0.41)	0.24 (0.12, 0.4)
CLF-14	0.33 (0.18, 0.53)	0.33 (0.18, 0.52)	0.33 (0.18, 0.52)	0.33 (0.18, 0.54)
CLF-12	0.02 (0, 0.09)	0.02 (0, 0.09)	0.02 (0, 0.09)	0.02 (0, 0.09)
CLF-11	0.35 (0.2, 0.55)	0.35 (0.2, 0.55)	0.35 (0.2, 0.55)	0.35 (0.2, 0.55)
CLF-10	0.21 (0.1, 0.37)	0.21 (0.09, 0.37)	0.21 (0.1, 0.37)	0.21 (0.1, 0.37)
CLF-9	0.09 (0.02, 0.21)	0.09 (0.02, 0.2)	0.09 (0.03, 0.2)	0.09 (0.02, 0.21)
CLF-8	0.02 (0, 0.09)	0.02 (0, 0.08)	0.02 (0, 0.09)	0.02 (0, 0.09)
CLF-7	0.17 (0.07, 0.32)	0.16 (0.07, 0.31)	0.17 (0.07, 0.31)	0.17 (0.07, 0.31)
CLF-6	0.14 (0.05, 0.28)	0.14 (0.05, 0.28)	0.14 (0.05, 0.28)	0.14 (0.05, 0.28)
CLF-5	0.24 (0.12, 0.4)	0.24 (0.11, 0.41)	0.24 (0.11, 0.41)	0.24 (0.11, 0.4)
CLF-4	0.12 (0.04, 0.23)	0.12 (0.04, 0.25)	0.12 (0.04, 0.24)	0.12 (0.04, 0.24)
CLF-3	0.17 (0.07, 0.31)	0.17 (0.07, 0.31)	0.17 (0.07, 0.31)	0.17 (0.07, 0.31)
CLF-2	0.12 (0.04, 0.24)	0.12 (0.04, 0.24)	0.12 (0.04, 0.25)	0.12 (0.04, 0.24)
CLF-1	0.12 (0.04, 0.24)	0.12 (0.04, 0.24)	0.12 (0.04, 0.24)	0.12 (0.04, 0.25)
CLF-LFE	0.09 (0.03, 0.2)	0.09 (0.02, 0.2)	0.09 (0.02, 0.2)	0.09 (0.03, 0.2)
CLF-LFER	0.07 (0.02, 0.16)	0.07 (0.02, 0.16)	0.07 (0.02, 0.16)	0.07 (0.02, 0.16)
CLF-R1	0.43 (0.26, 0.65)	0.43 (0.26, 0.65)	0.43 (0.25, 0.64)	0.42 (0.25, 0.65)
CLF-R2	0.16 (0.07, 0.31)	0.17 (0.07, 0.31)	0.17 (0.07, 0.3)	0.16 (0.07, 0.31)
CLF-R3	0.09 (0.03, 0.2)	0.09 (0.02, 0.21)	0.09 (0.03, 0.2)	0.09 (0.02, 0.2)
CLF-R4	0.02 (0, 0.09)	0.02 (0, 0.08)	0.02 (0, 0.08)	0.02 (0, 0.08)

Continued on next page

Camera	HMM(0.5)	HMM(1)	HMM(2)	MMMPP
CLF-R5	2.5 (0.24, 7.56)	1.5 (0.18, 4.41)	0.85 (0.09, 2.49)	4.51 (0.44, 14.5)
CLF-R6	0.99 (0.72, 1.32)	0.99 (0.71, 1.31)	0.99 (0.72, 1.32)	0.99 (0.72, 1.32)
CLF-R8	0.28 (0.15, 0.46)	0.28 (0.14, 0.47)	0.28 (0.15, 0.47)	0.29 (0.15, 0.47)
EA-A1	0.14 (0, 0.53)	0.14 (0, 0.53)	0.14 (0, 0.55)	0.14 (0, 0.51)
EA-A10	0.04 (0.01, 0.12)	0.04 (0, 0.12)	0.04 (0.01, 0.11)	0.04 (0.01, 0.12)
EA-A100	0.02 (0, 0.08)	0.02 (0, 0.08)	0.02 (0, 0.08)	0.02 (0, 0.08)
EA-B1	0.38 (0.23, 0.57)	0.38 (0.23, 0.58)	0.38 (0.22, 0.57)	0.38 (0.22, 0.59)
EA-B10	0.1 (0.03, 0.21)	0.11 (0.03, 0.21)	0.1 (0.03, 0.21)	0.11 (0.03, 0.21)
EA-B100	0.06 (0.01, 0.15)	0.06 (0.02, 0.15)	0.06 (0.01, 0.15)	0.06 (0.01, 0.15)
EA-C1	1.38 (1.12, 1.66)	1.38 (1.13, 1.66)	1.39 (1.14, 1.68)	1.38 (1.12, 1.65)
EA-C10	0.05 (0.01, 0.13)	0.05 (0.01, 0.13)	0.05 (0.01, 0.13)	0.05 (0.01, 0.13)
EA-C100	0.59 (0.38, 0.86)	0.59 (0.39, 0.85)	0.59 (0.39, 0.85)	0.59 (0.39, 0.85)
EA-D1	0.16 (0.07, 0.3)	0.16 (0.07, 0.31)	0.16 (0.06, 0.31)	0.16 (0.07, 0.3)
EA-D10	0.09 (0.03, 0.2)	0.09 (0.03, 0.2)	0.09 (0.02, 0.2)	0.09 (0.03, 0.2)
EA-D100	0.14 (0.05, 0.27)	0.14 (0.05, 0.27)	0.14 (0.05, 0.27)	0.14 (0.05, 0.27)
EA-E1	0.14 (0.05, 0.27)	0.14 (0.05, 0.27)	0.14 (0.05, 0.27)	0.14 (0.05, 0.28)
EA-E10	0.09 (0.03, 0.2)	0.09 (0.03, 0.2)	0.09 (0.03, 0.2)	0.09 (0.03, 0.2)
EA-E100	0.14 (0.05, 0.28)	0.14 (0.05, 0.27)	0.14 (0.05, 0.27)	0.14 (0.05, 0.27)
EA-F1	0.36 (0.2, 0.55)	0.36 (0.2, 0.57)	0.36 (0.2, 0.55)	0.35 (0.19, 0.55)
EA-F10	0.14 (0.05, 0.28)	0.14 (0.05, 0.27)	0.14 (0.05, 0.28)	0.14 (0.06, 0.28)
EA-F100	0.05 (0.01, 0.13)	0.05 (0.01, 0.14)	0.05 (0.01, 0.13)	0.05 (0.01, 0.14)
EA-R0	0.16 (0.07, 0.31)	0.17 (0.07, 0.31)	0.16 (0.06, 0.3)	0.17 (0.07, 0.31)
EA-R1	0.22 (0.1, 0.38)	0.21 (0.1, 0.38)	0.21 (0.09, 0.38)	0.21 (0.1, 0.38)
EA-R2	0.19 (0.09, 0.35)	0.19 (0.09, 0.35)	0.19 (0.09, 0.35)	0.19 (0.08, 0.35)
EA-R5	0.07 (0.01, 0.16)	0.07 (0.02, 0.17)	0.07 (0.01, 0.17)	0.07 (0.02, 0.16)
EA-R6	0.12 (0.04, 0.23)	0.12 (0.04, 0.24)	0.12 (0.04, 0.24)	0.11 (0.04, 0.23)
EA-R15	0.05 (0.01, 0.13)	0.05 (0.01, 0.14)	0.05 (0.01, 0.13)	0.05 (0.01, 0.13)
EA-R30	0.12 (0.04, 0.24)	0.12 (0.04, 0.24)	0.12 (0.04, 0.25)	0.12 (0.04, 0.24)
EA-R60	0.19 (0.08, 0.33)	0.19 (0.08, 0.34)	0.19 (0.08, 0.34)	0.19 (0.08, 0.34)
EA-R120	0.02 (0, 0.08)	0.02 (0, 0.08)	0.02 (0, 0.08)	0.02 (0, 0.08)
EA-VJR1(A)	0.38 (0.21, 0.61)	0.38 (0.21, 0.61)	0.38 (0.21, 0.61)	0.38 (0.21, 0.61)
EA-VJR2	0.09 (0.02, 0.2)	0.09 (0.03, 0.2)	0.09 (0.02, 0.19)	0.09 (0.02, 0.2)
EA-VJR3	7.17 (6.4, 8.01)	7.18 (6.41, 8.01)	7.18 (6.39, 8)	7.2 (6.35, 8.06)
EA-VJR4	0.05 (0.01, 0.13)	0.05 (0.01, 0.13)	0.05 (0.01, 0.13)	0.05 (0.01, 0.13)
EA-VJR5	0.27 (0.12, 0.48)	2.38 (1.88, 2.94)	0.28 (0.13, 0.5)	0.4 (0.21, 0.64)
EA-VJR6	0.14 (0.05, 0.28)	0.14 (0.05, 0.28)	0.14 (0.05, 0.28)	0.14 (0.05, 0.27)
EA-VJR7	3.8 (3.22, 4.42)	3.78 (3.22, 4.38)	3.78 (3.24, 4.41)	3.79 (3.23, 4.4)
EA-VJR8	0.06 (0.01, 0.16)	0.06 (0.01, 0.16)	0.06 (0.01, 0.16)	0.06 (0.01, 0.16)

Continued on next page

Camera	HMM(0.5)	HMM(1)	HMM(2)	MMMPP
EA-VJRR	0.11 (0.04, 0.23)	0.11 (0.03, 0.23)	0.11 (0.03, 0.23)	0.11 (0.03, 0.23)
OP-31	0.07 (0.01, 0.17)	0.07 (0.02, 0.17)	0.07 (0.01, 0.17)	0.07 (0.01, 0.17)
OP-29	1.61 (1.24, 2.01)	1.61 (1.25, 1.99)	1.61 (1.24, 2.02)	1.61 (1.24, 2.01)
OP-28	8.65 (7.76, 9.56)	8.61 (7.74, 9.51)	8.63 (7.79, 9.55)	8.65 (7.79, 9.53)
OP-27	0.28 (0.03, 0.84)	0.27 (0.02, 0.86)	0.26 (0.03, 0.84)	0.27 (0.03, 0.86)
OP-26 (A)	0.17 (0.06, 0.32)	0.17 (0.06, 0.33)	0.17 (0.06, 0.33)	0.17 (0.06, 0.33)
OP-26 (B)	2.91 (2.37, 3.51)	2.9 (2.36, 3.49)	2.9 (2.36, 3.49)	2.91 (2.36, 3.51)
OP-25	0.12 (0.01, 0.34)	0.11 (0.01, 0.32)	0.11 (0.01, 0.31)	0.12 (0.01, 0.33)
OP-24	0.73 (0.01, 3.6)	0.56 (0.01, 2.48)	0.32 (0, 1.43)	1.78 (0.01, 9.41)
OP-23	2.7 (2.34, 3.11)	2.69 (2.34, 3.1)	2.69 (2.34, 3.08)	2.69 (2.34, 3.07)
OP-22	0.28 (0.15, 0.46)	0.28 (0.14, 0.45)	0.27 (0.14, 0.45)	0.28 (0.14, 0.46)
OP-20	4.73 (4.08, 5.39)	4.71 (4.09, 5.39)	4.72 (4.11, 5.38)	4.73 (4.11, 5.38)
OP-19	0.32 (0.18, 0.52)	0.32 (0.18, 0.51)	0.32 (0.17, 0.51)	0.32 (0.17, 0.51)
OP-18	0.7 (0.48, 0.97)	0.7 (0.49, 0.95)	0.7 (0.48, 0.96)	0.7 (0.48, 0.96)
OP-16	0.31 (0.07, 0.76)	0.32 (0.07, 0.76)	0.29 (0.06, 0.68)	0.32 (0.07, 0.77)
OP-13	0.1 (0.01, 0.3)	0.1 (0.01, 0.3)	0.1 (0.01, 0.3)	0.1 (0.01, 0.28)
OP-12	8.54 (7.7, 9.43)	8.54 (7.68, 9.43)	8.54 (7.69, 9.44)	8.53 (7.69, 9.45)
OP-11	0.07 (0.02, 0.17)	0.07 (0.01, 0.18)	0.07 (0.01, 0.18)	0.07 (0.01, 0.17)
OP-10	0.31 (0.16, 0.49)	0.31 (0.17, 0.5)	0.31 (0.16, 0.5)	0.31 (0.16, 0.49)
OP-9	0.26 (0.13, 0.44)	0.26 (0.13, 0.43)	0.26 (0.13, 0.44)	0.26 (0.13, 0.44)
OP-8	0.45 (0.17, 0.87)	0.45 (0.18, 0.85)	0.48 (0.18, 0.9)	0.45 (0.17, 0.85)
OP-7	0.24 (0.01, 0.92)	0.27 (0.01, 1.02)	0.21 (0, 0.81)	0.24 (0.01, 0.94)
OP-6	0.81 (0.56, 1.1)	0.81 (0.56, 1.08)	0.81 (0.56, 1.11)	0.82 (0.57, 1.11)
OP-5	2.27 (1.82, 2.74)	2.26 (1.84, 2.72)	2.26 (1.84, 2.74)	2.27 (1.84, 2.75)
OP-4	2.45 (2.01, 2.94)	2.45 (1.99, 2.94)	2.44 (2, 2.94)	2.44 (2, 2.91)
OP-2	0.31 (0.06, 0.77)	0.32 (0.07, 0.82)	0.33 (0.07, 0.82)	0.3 (0.06, 0.74)
OP-1	1.62 (0.7, 2.97)	1.5 (0.63, 2.72)	1.27 (0.51, 2.34)	0.94 (0.26, 2.07)
OP-OP2	0.13 (0.05, 0.25)	0.13 (0.05, 0.26)	0.13 (0.05, 0.26)	0.13 (0.05, 0.26)
OP-OP3	1.01 (0.48, 1.75)	1.02 (0.47, 1.8)	0.95 (0.43, 1.62)	0.98 (0.42, 1.71)
OPF-10	0.49 (0.23, 0.86)	0.48 (0.22, 0.84)	0.49 (0.23, 0.86)	0.49 (0.21, 0.87)
OPF-8	8.03 (7.14, 8.92)	7.96 (7.07, 8.9)	7.93 (7.07, 8.87)	8.14 (7.22, 9.12)
OPF-7	0.05 (0.01, 0.13)	0.05 (0.01, 0.13)	0.05 (0, 0.13)	0.05 (0.01, 0.13)
OPF-6	0.14 (0.05, 0.28)	0.14 (0.06, 0.28)	0.14 (0.05, 0.27)	0.14 (0.05, 0.28)
OPF-4	0.19 (0.08, 0.34)	0.19 (0.08, 0.35)	0.19 (0.08, 0.34)	0.19 (0.09, 0.35)
OPF-3	0.64 (0.42, 0.91)	0.64 (0.42, 0.9)	0.64 (0.42, 0.9)	0.64 (0.42, 0.91)
OPF-2	0.17 (0.07, 0.31)	0.16 (0.07, 0.31)	0.17 (0.07, 0.31)	0.17 (0.07, 0.31)
OPF-1	0.26 (0.13, 0.43)	0.26 (0.13, 0.43)	0.26 (0.13, 0.42)	0.26 (0.13, 0.42)
OPF-HCV1	0.21 (0.1, 0.37)	0.21 (0.1, 0.37)	0.21 (0.1, 0.37)	0.21 (0.09, 0.37)

Continued on next page

Camera	HMM(0.5)	HMM(1)	HMM(2)	MMMPP
OPF-HCV2	0.09 (0.03, 0.21)	0.09 (0.03, 0.21)	0.1 (0.03, 0.21)	0.1 (0.03, 0.21)
OPF-HCV3	0.38 (0.21, 0.58)	0.38 (0.22, 0.59)	0.38 (0.21, 0.58)	0.38 (0.22, 0.59)
OPF-HCV4	0.12 (0.04, 0.23)	0.12 (0.04, 0.24)	0.12 (0.04, 0.23)	0.12 (0.04, 0.25)
OPF-HCV5	0.31 (0.17, 0.5)	0.31 (0.17, 0.51)	0.31 (0.17, 0.5)	0.31 (0.16, 0.49)
OPF-HCV6	0.93 (0.66, 1.25)	0.93 (0.66, 1.24)	0.93 (0.66, 1.24)	0.93 (0.67, 1.25)
OPF-HCV7	0.14 (0.05, 0.28)	0.14 (0.05, 0.28)	0.14 (0.05, 0.28)	0.14 (0.05, 0.28)
OPF-HCV8	0.33 (0.18, 0.52)	0.33 (0.18, 0.52)	0.33 (0.19, 0.53)	0.33 (0.18, 0.53)
OPF-HCV9	0.13 (0.03, 0.3)	0.13 (0.03, 0.32)	0.13 (0.03, 0.32)	0.13 (0.03, 0.31)
OPF-HCV11	0.19 (0.08, 0.33)	0.19 (0.08, 0.34)	0.19 (0.08, 0.36)	0.19 (0.09, 0.34)
OPF-HCV12	0.21 (0.03, 0.62)	0.22 (0.03, 0.64)	0.22 (0.03, 0.64)	0.2 (0.02, 0.6)
OPF-HCV13	0.31 (0.17, 0.5)	0.31 (0.16, 0.49)	0.31 (0.17, 0.49)	0.31 (0.16, 0.49)
OPF-HCV15	0.07 (0.02, 0.14)	0.07 (0.02, 0.14)	0.07 (0.02, 0.14)	0.07 (0.02, 0.14)
OPF-R1	0.07 (0.02, 0.17)	0.07 (0.02, 0.17)	0.07 (0.02, 0.17)	0.07 (0.01, 0.17)
OPF-R2	0.02 (0, 0.09)	0.02 (0, 0.09)	0.02 (0, 0.08)	0.02 (0, 0.09)
OPF-R4	0.27 (0.14, 0.46)	0.27 (0.14, 0.46)	0.27 (0.14, 0.46)	0.28 (0.14, 0.46)
OPF-R5	0.11 (0, 0.42)	0.12 (0, 0.46)	0.11 (0, 0.43)	0.11 (0, 0.42)
OPF-R6	0.19 (0.09, 0.33)	0.19 (0.09, 0.34)	0.19 (0.09, 0.33)	0.19 (0.09, 0.33)
OPF-RR2	1.06 (0.02, 4.42)	0.7 (0.02, 2.82)	0.38 (0.01, 1.49)	1.03 (0.01, 4.19)
OPF-RR3	0.07 (0.01, 0.16)	0.07 (0.02, 0.17)	0.07 (0.01, 0.17)	0.07 (0.01, 0.17)
OPF-RR7	0.05 (0.01, 0.13)	0.05 (0.01, 0.13)	0.05 (0.01, 0.13)	0.05 (0.01, 0.13)
OPF-RR14	0.83 (0.58, 1.13)	0.83 (0.58, 1.11)	0.83 (0.59, 1.11)	0.83 (0.58, 1.12)
OPF-RR16	0.25 (0.03, 0.74)	0.25 (0.03, 0.73)	0.22 (0.02, 0.64)	0.26 (0.03, 0.73)
λ_3^-	895 (858, 933)	1083(1037,1129)	746 (716,777)	1069(1025,1113)

References

L. Bahaa-el din, R. Sollmann, L. T. Hunter, R. Slotow, D. W. Macdonald, and P. Henschel. Effects of human land-use on africa's only forest-dependent felid: The african golden cat caracal aurata. *Biological Conservation*, 199:1–9, 2016. ISSN 0006-3207. doi: https://doi.org/10.1016/j.biocon.2016.04.013. URL `https://www.sciencedirect.com/science/article/pii/S0006320716301495`.

D. L. Borchers and R. Langrock. Double-observer line transect surveys with markov-modulated poisson process models for animal availability. *Biometrics*, 71(4):1060–1069, 2015. ISSN 0006-341X. doi: 10.1111/biom.12341. URL `https://dx.doi.org/10.1111/biom.12341`.

J. W. Bubnicki, B. Norton, S. J. Baskauf, T. Bruce, F. Cagnacci, J. Casaer, M. Churski, J. P. G. M. Cromsigt, S. D. Farra, C. Fiderer, and et al. Camtrap dp: an open standard for the fair exchange and archiving of camera trap data. *Remote Sensing in Ecology and Conservation*, 10(3):283–295, 2024. ISSN 2056-3485. doi: 10.1002/rse2.374.

R. Buckreus, C. P. Smith, and M. Kisacikoglu. Development of a hybrid energy management solution for an outdoor trail camera. *IEEE Transactions on Industrial Electronics*, 68(11):10959–10969, 2021. ISSN 0278-0046. doi: 10.1109/tie.2020.3034854.

A. C. Burton, E. Neilson, D. Moreira, A. Ladle, R. Steenweg, J. T. Fisher, E. Bayne, and S. Boutin. Review: Wildlife camera trapping: a review and recommendations for linking surveys to ecological processes. *Journal of Applied Ecology*, 52(3):675–685, 2015. ISSN 0021-8901. doi: 10.1111/1365-2664.12432.

R. Choquet. Markov-modulated poisson processes as a new framework for analysing capture–recapture data. *Methods in Ecology and Evolution*, 9(4):929–935, 2018. ISSN 2041-210X. doi: 10.1111/2041-210x.12961.

C. P. Cordier, D. A. Ehlers Smith, Y. Ehlers Smith, and C. T. Downs. Camera trap research in africa: A systematic review to show trends in wildlife monitoring and its value as a research tool. *Global Ecology and Conservation*, 40:e02326, 2022. ISSN 2351-9894. doi: https://doi.org/10.1016/j.gecco.2022.e02326. URL `https://www.sciencedirect.com/science/article/pii/S2351989422003286`.

P. de Valpine, D. Turek, C. Paciorek, C. Anderson-Bergman, D. Temple Lang, and R. Bodik. Programming with models: writing statistical algorithms for general model structures with NIMBLE. *Journal of Computational and Graphical Statistics*, 26:403–413, 2017. doi: 10.1080/10618600.2016.1172487.

R. L. Emmet, R. A. Long, and B. Gardner. Modeling multi-scale occupancy for monitoring rare and highly mobile species. *Ecosphere*, 12(7), 2021. ISSN 2150-8925. doi: 10.1002/ecs2.3637.

W. W. Fund. 2024 living planet report, 2024. URL `https://www.worldwildlife.org/publications/2024-living-planet-report`. Accessed: 2026-03-03.

G. García-Salgado, S. Rebollo, L. Pérez-Camacho, S. Martínez-Hesterkamp, A. Navarro, and J.-M. Fernández-Pereira. Evaluation of trail-cameras for analyzing the diet of nesting raptors using the northern goshawk as a model. *PLOS One*, 10(5):e0127585, 2015. ISSN 1932-6203. doi: 10.1371/journal.pone.0127585. URL `https://dx.doi.org/10.1371/journal.pone.0127585`.

P. Glover-Kapfer, C. A. Soto-Navarro, and O. R. Wearn. Camera-trapping version 3.0: current constraints and future priorities for development. *Remote Sensing in Ecology and Conservation*, 5(3):209–223, 2019. ISSN 2056-3485. doi: 10.1002/rse2.106.

A. Gonzalez, P. Vihervaara, P. Balvanera, A. E. Bates, E. Bayraktarov, P. J. Bellingham, A. Bruder, J. Campbell, M. D. Catchen, J. Cavender-Bares, et al. A global biodiversity observing system to unite monitoring and guide action. *Nature Ecology & Evolution*, 7(12):1947–1952, 2023.

F. B. Gonçalves, L. M. Dutra, and R. W. C. Silva. Exact and computationally efficient bayesian inference for generalized markov modulated poisson processes. *Statistics and Computing*, 32(1), 2022. ISSN 0960-3174. doi: 10.1007/s11222-021-10074-y.

G. Guillera-Arroita, B. J. T. Morgan, M. S. Ridout, and M. Linkie. Species occupancy modeling for detection data collected along a transect. *Journal of Agricultural, Biological, and Environmental Statistics*, 16(3):301–317, 2011. ISSN 1085-7117. doi: 10.1007/s13253-010-0053-3.

K. F. Kellner, A. W. Parsons, R. Kays, J. J. Millspaugh, and C. T. Rota. A two-species occupancy model with a continuous-time detection process reveals spatial and temporal interactions. *Journal of Agricultural, Biological and Environmental Statistics*, 27(2):321–338, 2022. ISSN 1085-7117. doi: 10.1007/s13253-021-00482-y.

Y. Luo and C. Sherlock. Bayesian inference for the markov-modulated poisson process with an outcome process. *Journal of the Royal Statistical Society Series C: Applied Statistics*, 74(5):1239–1254, 03 2025. ISSN 0035-9254. doi: 10.1093/jrsssc/qlaf021. URL `https://doi.org/10.1093/jrsssc/qlaf021`.

B. T. Mcclintock, R. Langrock, O. Gimenez, E. Cam, D. L. Borchers, R. Glennie, and T. A. Patterson. Uncovering ecological state dynamics with hidden markov models. *Ecology Letters*, 23(12):1878–1903, 2020. ISSN 1461-023X. doi: 10.1111/ele.13610.

T. McIntyre, T. L. Majelantle, D. J. Slip, and R. G. Harcourt. Quantifying imperfect camera-trap detection probabilities: implications for density modelling. *Wildlife Research*, 47(2):177–185, 02 2020. ISSN 1035-3712. doi: 10.1071/WR19040. URL `https://doi.org/10.1071/WR19040`.

P. D. Meek, G. Ballard, A. Claridge, R. Kays, K. Moseby, T. O'Brien, A. O'Connell, J. Sanderson, D. E. Swann, M. Tobler, and et al. Recommended guiding principles for reporting on camera trapping research. *Biodiversity and Conservation*, 23(9):2321–2343, 2014. ISSN 0960-3115. doi: 10.1007/s10531-014-0712-8.

S. Mews, B. Surmann, L. Hasemann, and S. Elkenkamp. Markov-modulated marked poisson processes for modeling disease dynamics based on medical claims data. *Statistics in Medicine*, 42(21):3804–3815, 2023. ISSN 0277-6715. doi: 10.1002/sim.9832.

Y. Nakashima, S. Hongo, K. Mizuno, G. Yajima, and Z. C. B. Dzefck. Double-observer approach with camera traps can correct imperfect detection and improve the accuracy of density estimation of unmarked animal populations. *Scientific Reports*, 12(1), 2022. ISSN 2045-2322. doi: 10.1038/s41598-022-05853-0.

J. D. Nichols, L. L. Bailey, A. F. O'Connell Jr., N. W. Talancy, E. H. Campbell Grant, A. T. Gilbert, E. M. Annand, T. P. Husband, and J. E. Hines. Multi-scale occupancy estimation and modelling using multiple detection methods. *Journal of Applied Ecology*, 45(5):1321–1329, 2008. ISSN 0021-8901. doi: 10.1111/j.1365-2664.2008.01509.x. URL `https://dx.doi.org/10.1111/j.1365-2664.2008.01509.x`.

P. Palencia, J. Vicente, R. C. Soriguer, and P. Acevedo. Towards a best-practices guide for camera trapping: assessing differences among camera trap models and settings under field conditions. *Journal of Zoology*, 316(3):197–208, 2022. ISSN 0952-8369. doi: 10.1111/jzo.12945.

L. Pautrel, S. Moulherat, O. Gimenez, and M. Etienne. Analysing biodiversity observation data collected in continuous time: Should we use discrete- or continuous-time occupancy models? *Methods in Ecology and Evolution*, 2024. ISSN 2041-210X. doi: 10.1111/2041-210x.14314.

N. Priyadarshani, S. Marsland, and I. Castro. Automated birdsong recognition in complex acoustic environments: a review. *Journal of Avian Biology*, 49(5):jav–01447, 2018. ISSN 0908-8857. doi: 10.1111/jav.01447.

R Core Team. *R: A Language and Environment for Statistical Computing*. R Foundation for Statistical Computing, Vienna, Austria, 2025. URL `https://www.R-project.org/`.

M. S. Ridout and M. Linkie. Estimating overlap of daily activity patterns from camera trap data. *Journal of Agricultural, Biological and Environmental Statistics*, 14(3):322–337, 2009. ISSN 1085-7117. doi: 10.1198/jabes.2009.08038.

M. R. Schofield, R. J. Barker, and N. Gelling. Continuous-time capture–recapture in closed populations. *Biometrics*, 74(2):626–635, 2018. doi: https://doi.org/10.1111/biom.12763. URL `https://onlinelibrary.wiley.com/doi/abs/10.1111/biom.12763`.

R. Steenweg, M. Hebblewhite, R. Kays, J. Ahumada, J. T. Fisher, C. Burton, S. E. Townsend, C. Carbone, J. M. Rowcliffe, J. Whittington, and et al. Scaling-up camera traps: monitoring the planet's biodiversity with networks of remote sensors. *Frontiers in Ecology and the Environment*, 15(1):26–34, 2017. ISSN 1540-9295. doi: 10.1002/fee.1448. URL `https://dx.doi.org/10.1002/fee.1448`.

T. Zett, K. J. Stratford, and F. J. Weise. Inter-observer variance and agreement of wildlife information extracted from camera trap images. *Biodiversity and Conservation*, 31(12):3019–3037, 2022. ISSN 0960-3115. doi: 10.1007/s10531-022-02472-z.

W. Zucchini and I. L. MacDonald. *Hidden Markov models for time series: an introduction using R*. Chapman and Hall/CRC, 2009.